UNIVERSITAT POLITÈCNICA DE CATALUNYA
BARCELONATECH
Escola Tècnica Superior d'Enginyeria
de Telecomunicació de Barcelona

telecos
BCN

ENGINEERING PHYSICS

BACHELOR'S THESIS

Weak Value Amplification and Hong-Ou-Mandel effect for quantum sensing

Anna Migó Lluís

June 2021

Directed by

Dr. Juan P. Torres, UPC

Acknowledgements

Many thanks to whom either directly or indirectly has helped me go through the process of issuing this thesis.

I want to thank firstly the administration and staff at ICFO (The Institute of Photonic Sciences) for providing me the best they could during this semester. Also, I thank Daniel Urriego that helped me through the process.

Especially, to Prof. Juan P. Torres for being the main reason why this project could be possible and for his kind supervision and support. I am deeply grateful.

Abstract

The use of new states of light (quantum sensing and quantum imaging) has opened the door to new protocols for parameter estimation with enhanced resolution. In this project we study two techniques that allow increasing the resolution of measurements, allowing the detection of extremely small changes in variables. In one case, when resolution is limited by technical noise, the protocol is Weak Value Amplification (WVA). In the second case we make use of quantum interference and develop a new type of microscope (Quantum Differential Interference Contrast, QDIC) that does phase retrieval based on the Hong-Ou-Mandel effect. We consider phase objects, such as sub-wavelength gratings and cliff-like structures, to show the capabilities and potential of the techniques considered.

Contents

1 Introduction

The aim of experimental science is always to look for the limits that exist in the measurements. There are two main kinds of limits:

1. Fundamental. For instance, the accuracy of determining a phase of a photon set to a single-mode coherent quantum state is $\sqrt{\langle(\Delta\phi)^2\rangle} \sim 1/\sqrt{N}$ because of the statistical nature of the light beam. This determines the ultimate limit to the sensitivity achievable [1].

2. Technical noise. For instance, the noise added in the detection stage might make it impossible to distinguish two relative values of the physical quantity of interest, effectively limiting the measurement's sensitivity beyond what any more fundamental limit can restrict.

In this report, we focus on two main techniques to increase the resolution of measurements of extremely small quantities.

The first one is Weak Value Amplification (WVA). It was proposed by Aharonov, Albert, and Vaidman, published in Physical Review Letters. Since its birth in 1988 [2], its usefulness has been demonstrated in numerous scenarios under a great variety of experimental conditions [3], [4] and [5]. It is based on two main ingredients: first, the existence of a weak interaction that couples the properties of the system with individual degrees of freedom; secondly, the measurement of the mean value of abnormally large pointer states, after the appropriate system state selection before and after.

It appears to be an exciting line of research that could result in improved quantum sensing technology. In particular, the research group "Quantum Engineering of Light" from ICFO (The Institute of Photonic Sciences) led by Prof. Dr. Juan P. Torres demonstrated a few years ago that minimal temporal delays, about the order of femtosecond, between pulses much smaller than their pulse width, could be measured using this method [6].

The second one relies on the Hong-Ou-Mandel effect (HOM). This effect of quantum optics is a two-photon interference result demonstrated in 1987 to measure subpicosecond time intervals between two photons [7]. Its full generality can help detect any other difference like frequency shifts or other changes in the wave function.

Imagine two photons in a specific state that are about to cross a beam splitter, each of them can take two paths, up and down. We also place two detectors, one up and one down. Each can "click" (find the photon) with a probability 1/2. When these two detectors D_1 and D_2 click simultaneously, we say there is a coincidence. If we have two indistinguishable input photon states, then, due to interference, both photons leave the beam splitter through the same port. Both detectors have an equal probability of clicking,

but the number of coincidences becomes zero (it is explained in detail in [8]).

The HOM effect will be combined with the Differential Interference Contrast (DIC) technique, obtaining the Quantum Differential Interference Contrast (QDIC). DIC was developed by Polish physicist Georges Nomarski in 1952 [9] and works on the principle of interferometry to gain information about the optical path length of the sample. Interferometers are based on splitting into two beams the light from a single source. These two travel in different optical paths and then are combined again to produce interference. The resulting interference fringes give information about the difference in optical path lengths so that one can measure phase shifts $\Delta\phi$. In the QDIC, the HOM will be used at the end of the setup, and will measure the distinguishability of the two photons, so that it is very sensitive to differences between the photons that interfere (such as polarization, a temporal delay, or spatial shape).

Phase objects are samples that change the phase but not the light wave amplitude. This report will work with sub-wavelength gratings (in particular, we will consider the 1D Lamellar z-periodic dielectric waveguide structure) and edge structures (mainly described as step functions). We refer to a sub-wavelength grating when the diffraction effects are suppressed for all orders$\geq$ 1, and this happens for small pitches of the grating, as the condition is that the wavelength used divided by pitch must be higher than the more significant index of refraction considered [10]. The parameters to study will be both the duty cycle D and the period Λ. As for the edge structures, we will be interested basically in the height of the step d.

Our goal is mainly to apply these two techniques to retrieve information of the previous mentioned types of phase object by detecting tiny changes of certain physical quantities of interest:

- With Weak Value Amplification, we will translate the physical properties of the phase objects into frequency-shifted pulses. The technique will allow us to measure extremely small temporal delays between two pulses much longer than the delay to be measured. It is based on the measurement of the spectra.
- With the Quantum Interference Differential Contrast based on the Hong-Ou-Mandel effect, we will translate the physical properties of the phase objects into polarization states. It is based on the measurement of quantum distinguishability.

Finally, part of the study has been a theoretical framework for two incoming projects of the research group "Quantum Engineering of Light" from ICFO (The Institute of Photonic Sciences) led by Prof. Dr. Juan P. Torres. For starters, we are testing the ground for retrieving information from a sub-wavelength grating through Weak Value Amplification in the laboratory. In the second place, we keep investigating to do an experimental study

on the Quantum Differential Interference Contrast, which is currently going on.

2 What is Weak Value Amplification (WVA)

A *weak value* is a quantity related to a shift of the usual measuring procedure for pre-selection and post-selection ensembles of quantum systems. It was first defined by Yakir Aharonov, David Albert, and Lev Vaidman, published in Physical Review Letters 1988 [2]. They found that under some natural conditions of the weakness of the measurement, its result consistently defines a new kind of value for a quantum variable, which they called the *weak value*. These same authors suggested *weak values* could be used in quantum metrology [4], [5] (the study of making a high resolution and susceptible measurements of physical parameters). This suggestion was followed by Hosten and Kwiat [11] and later by Dixon [12]. It appears to be an exciting line of research that could result in improved quantum sensing technology. Furthermore, in 2011 weak measurements of many photons prepared in the same pure state, followed by solid measurements of a complementary variable, were used to perform quantum tomography (i.e., reconstruct the state in which the photons were prepared)[13].

So that Weak Value Amplification is a solution to improving the ultimate resolution of a detection system with sensitivity limits given by technical noise, as the method increases it by effectively lowering the value of the smallest quantity that can be detected. Notice that with this technique, a small fraction of the photons is used, so the signal is received in the detector with much less intensity because of the quasi-orthogonality of the input and output polarization states selected.

In general, a WVA scheme requires three main ingredients [14]: 1) the consideration of two subsystems that are weakly coupled; 2) the pre-selection of the input states of both subsystems; and 3) the post-selection of the state in one of the subsystems and the measurement of the state of the remaining subsystem. This technique will be used to reveal tiny changes of a variable of interest, specifically; in this report, we will be working with the introduction of a tiny temporal delay T due to large bandwidth pulses.

Also, this technique gives us more extended data than the standard measurements through polarization. Working with frequencies allow us to obtain a frequency shift Δf, as we can integrate this added degree of freedom, instead of just retrieving the losses obtained when projecting onto a known polarized state.

2.1 Measurement of extremely small temporal delays

2.1.1 General expression

We consider the specific scheme proposed by Salazar-Serrano, Luis José and Torres seen in [6] to measure minimal time delays T between 2 beams with orthogonal polarizations with the help of optical pulses characterized by a time duration much larger than this

delay introduced, $T << \tau$. It is based on an interference effect in the frequency domain generated with WVA, which produces a measurable shift of the central frequency of the beam.

In this experiment, there are two degrees of freedom intervening: the polarization and the spectrum of the optical beam characterized with a time duration τ. The objective is to choose an appropriate pre-selection and post-selection of the polarization of the output light so that an anomalously significant shift generated by tiny changes of the time delay can be detected when measuring the spectrum of the beam. The polarization-dependent temporal delay will be introduced with the help of the Michelson interferometer so that, for sake of simplicity and facility when analysing the results, the setup makes use of linear optics elements only. The specific weak amplification scheme considered is depicted in Figure 1.

To begin with, consider an unpolarized light source characterized with a large beam width τ and a spectral density $S_{in}(\Omega) = 2\varepsilon_0 c|E_{in}(\Omega)|^2$. In the pre-selection stage is defined the polarization state to work with so that this initial unpolarized light source is converted into a left-handed circular polarized light $\widehat{e}_{in} = 1/\sqrt{2}(\widehat{H} - i\widehat{V})$.

Afterward, the Michelson interferometer creates a delay between both horizontal $\widehat{H}$ and vertical $\widehat{V}$ polarizations. Then, it starts separating both components and introducing different phases in each of them $\phi_i = (\omega_0 + \Omega)T_i$ where the temporal delay depends on the distance the movable mirror is placed from the QWP, $T_i = 2d_i/c$ (see Figure 1). After this stage painted in pink, the electric field obtained after passing through the PBS is the following:

$$E_1(\Omega) = \frac{E_{in}(\Omega)}{\sqrt{2}} \left(\widehat{H} + \widehat{V} \exp\left[-i(\omega_0 + \Omega)T + i\frac{\pi}{2} \right] \right) e^{i\phi} \tag{2.1}$$

where $T = T_1 - T_2$. Notice that there are an exponential term $e^{i\phi}$ that corresponds to $e^{-i(\omega_0+\Omega)T_1} e^{-i\frac{\pi}{2}}$, but it is not essential, as it can be omitted because it is just a global phase and it has no distinguishable effect between the states.

Finally, in the post-selection stage, the field obtained in Equation 2.1 is projected into a state given by the polarization vector $\widehat{e}_{out} = 1/\sqrt{2}(\widehat{H} + e^{i\Gamma}\widehat{V})$. Therefore, at the output one obtains the following electric field:

$$E_{out}(\Omega) = \frac{E_{in}(\Omega)}{2} \left(1 + \exp\left[i(\omega_0 + \Omega)T - i(\Gamma + \frac{\pi}{2}) \right] \right) \tag{2.2}$$

With this obtained expression, one can easily see that the post-selection angle must be chosen carefully. Considering a tiny delay T, for $\Gamma = -\frac{\pi}{2}$ the input and output polarization states almost coincide, as $\widehat{e}_{out} \sim |L\rangle$, while for $\Gamma = \frac{\pi}{2}$ they will be nearly orthogonal, as $\widehat{e}_{out} \sim |R\rangle$.

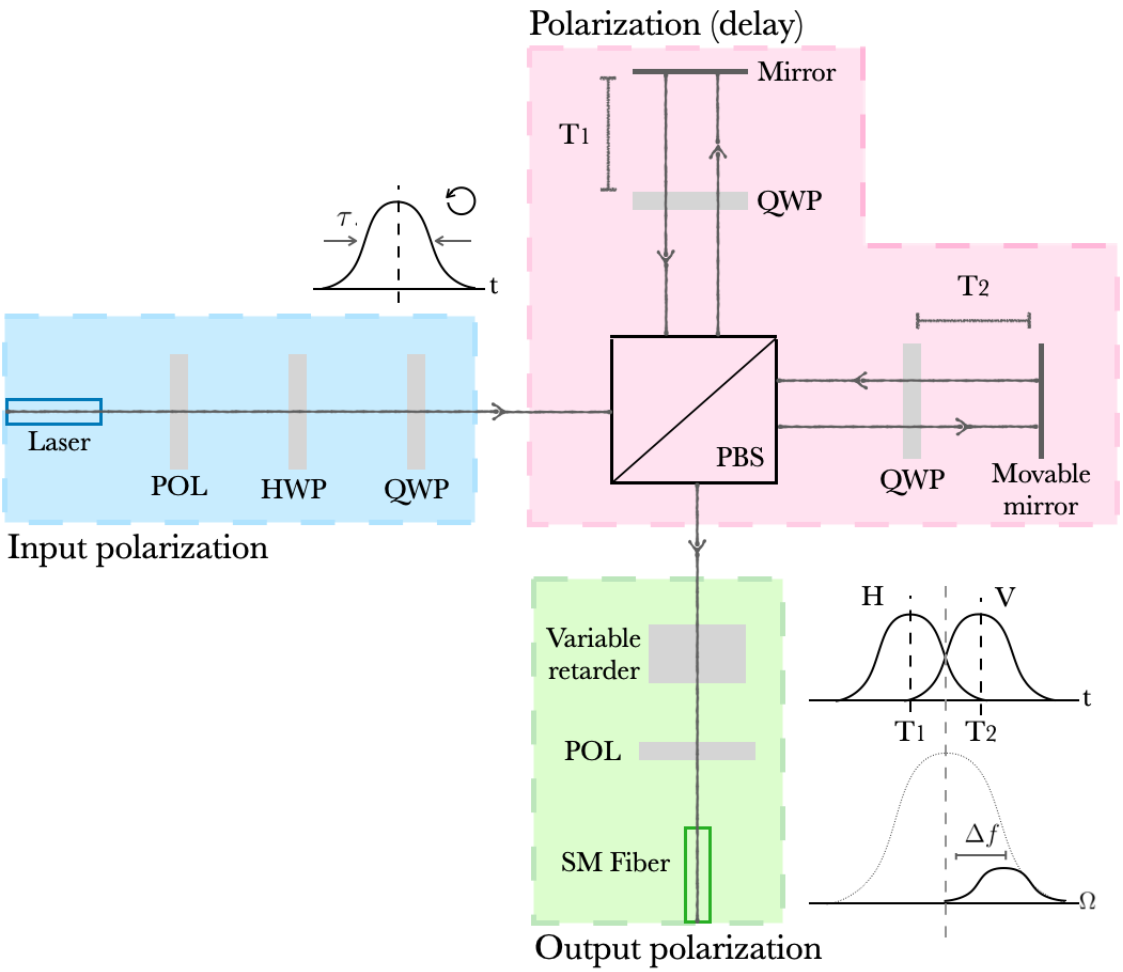

Figure 1. **Weak Value Amplification scheme aimed at detecting extremely small temporal delays**. In blue the pre-selection stage, polarization input state-defined: a $-45°$ linear polarizer, a $\frac{\lambda}{2}$ wave plate (HWP) and a $\frac{\lambda}{4}$ wave plate (QWP) force the input optical beam into a state of polarization left-handed circular. In pink, the weak coupling stage, the introduction of a polarization-dependent delay: A Michelson-Morley interferometer, composed of a polarizing beam splitter (PBS), two $\frac{\lambda}{4}$ wave plates (QWP), and two mirrors, divides the input beam into two beams, with equal power and with orthogonal polarizations, that travel through different paths of the interferometer. Each mirror is mounted in a translation stage that allows changing the temporal delay in each path ($T_1 - T_2 = T$). In green the post-selection stage, polarization output state-defined: a variable retarder (defined by Γ) followed by a $45°$ polarizer. Finally, the output beam is focused in a single-mode fiber (SM), and its spectrum is measured with an optical spectrum analyzer (OSA).

The interesting measure, though, is the output spectral density, so once the electric field has been found, the analytical expression can be easily derived, obtaining:

$$S_{out}(\Omega) = \frac{S_{in}(\Omega)}{2}\left(1 + \cos\left((\omega_0 + \Omega)T - \Gamma - \pi/2\right)\right) \tag{2.3}$$

Finally, in order to characterize the output spectrum, the frequency shift, wavelength shift, and insertion loss can be obtained as a function of the post-selection angle Γ:

$$\Delta f(\Gamma) = \frac{1}{2\pi}\frac{\int d\Omega\ S_{out}(\Omega)\Omega}{\int d\Omega\ S_{out}(\Omega)};\ \ \Delta\lambda(\Gamma) = \frac{\lambda^2}{2\pi c}\Delta f(\Gamma) \tag{2.4}$$

$$L(\Gamma) = -10\log\frac{\int d\Omega\ S_{out}(\Omega)}{\int d\Omega\ S_{in}(\Omega)} \tag{2.5}$$

The frequency shift provides information on how much the signal has moved from the center in the frequency regime, retrieving information about the temporal delay T introduced by the interferometer. Notice that it has been normalized. Either way, instead of working with frequency [Hz] is better to talk about wavelength units because it is a much more helpful and standard reference. On the other hand, the transformation from Δf to $\Delta\lambda$ is valid because the order of the wavelength shift is nanometers, a minimal magnitude. It is also essential to measure the insertion losses as it is in our best interest to know how much signal has been lost.

Let us review what would have happened if we have used the standard retrieval with polarization: starting with the same conditions, with a left-handed circular polarized state, and introducing the same delay through the SWG, we would project the obtained state onto the known orthogonal state $\widehat{R}$:

$$\widehat{E}_1 = \frac{1}{\sqrt{2}}\big(\widehat{H} - ie^{i\omega_0 T}\widehat{V}\big) = \frac{1}{2}\left((1 - e^{i\omega_0 T})\widehat{R} + (1 + e^{i\omega_0 T})\widehat{L}\right) \tag{2.6}$$

$$S_{out} = \big|\ \langle\widehat{E_1}\big|\widehat{R}\rangle\ \big|^2 = \frac{1}{2}(1 - \cos\omega_0 T) \tag{2.7}$$

The only information obtained, therefore, are the losses.

2.1.2 Gaussian pulse with a Gaussian spectrum

In most cases of interest, a Gaussian pulse with a Gaussian spectrum can be a good approximation, and it will allow us to obtain handy expressions to analyze data. Therefore, the input optical beam is considered to have a Gaussian spectrum characterized with a carrier wave ω_0, no chirp, and a beam temporal width $\tau_{FWHM} = \tau$. The normalized input

electric field in the time domain reads:

$$E_{in}(t) = E_{0t} \exp\left[-2\ln 2\frac{t^2}{\tau^2} + i\omega_0 t\right], \text{ where } E_{0t} = \left(\frac{4\ln 2}{\pi\tau^2}\right)^{1/4} \tag{2.8}$$

It can be easy to transform the time domain into a frequency domain using the Fourier transform (FT), $F(\Omega) = \int dt\, f(t) \exp\left[-i(\Omega + \omega_0)t\right]$, obtaining the following expression (See the development in Appendix A):

$$E_{in}(\Omega) = E_{0\Omega} \exp\left[-\frac{\tau^2}{8\ln 2}\Omega^2\right], \text{ where } E_{0\Omega} = \left(\frac{\tau^2}{4\pi\ln 2}\right)^{1/4} \tag{2.9}$$

Moreover, once again the input spectral density can be easily derived, as it is proportional to the squared electric field ($S_{in}(\Omega) = 2\epsilon_0 c|E_{in}(\Omega)|^2$):

$$S_{in}(\Omega) = S_{0\Omega} \exp\left[-\frac{\tau^2}{4\ln 2}\Omega^2\right], \text{ where } S_{0\Omega} = \frac{\tau\epsilon_0 c}{\sqrt{\pi\ln 2}} \tag{2.10}$$

Now it just has to be inserted into Equation 2.3 so that the output spectral density reads:

$$S_{out}(\Omega) = \frac{S_{0\Omega}}{2} e^{-\frac{\tau^2}{4\ln 2}\Omega^2}\left(1 + \cos\left((\Omega + \omega_0)T - \Gamma - \pi/2\right)\right) \tag{2.11}$$

Finally, both frequency shift and insertion losses can now be calculated using Equations 2.4 and 2.11 (see the mathematical development in Appendix A):

$$\Delta f(\Gamma) = -\frac{\ln 2}{\pi}\left(\frac{T}{\tau^2}\right)\frac{\gamma\sin(\omega_0 T - \Gamma - \pi/2)}{\gamma\cos(\omega_0 T - \Gamma - \pi/2) + 1} \tag{2.12}$$

$$L(\Gamma) = -10\log\left[\frac{1}{2}\left(1 + \gamma\cos(\omega_0 T - \Gamma - \pi/2)\right)\right] \tag{2.13}$$

where

$$\gamma = \exp\left[-\ln 2\frac{T^2}{\tau^2}\right] \tag{2.14}$$

Notice that for a post-selection angle $\Gamma_0 = \omega_0 T + \frac{\pi}{2}$, the frequency shift will be zero, $\Delta f(\Gamma_0) = 0$ and there will be maximum insertion losses, which makes total sense as it will be the almost orthogonal state.

2.1.3 Main results

For the sake of clarity, the same fiber laser will be used during the whole report. The optical beam will be centered at a wavelength $\lambda_0 = 810$nm, corresponding to a central frequency of $\omega_0 = 2327.1THz$, and will have a bandwidth $\Delta\lambda = 30$nm. Instead of

characterizing the Gaussian beam with a concrete beam duration, which could be for example $\tau = 100$fs and would necessarily force the use of a coherent laser, it will be defined as $\tau = \frac{\lambda^2}{2\pi c}\frac{1}{\Delta\lambda} = 11.6$fs. In order to prove how small is the temporal delay that can be retrieved with the WVA technique, a temporal delay of $T = 10$as will be introduced.

One can distinguish two different regimes depending on what post-selection angle is used:

1. The **low-loss regime**. It is located around the output state with a polarization almost parallel to the polarization of the input signal, in our case would be the left-handed circular state $|L\rangle$, which entails a Γ around $\Gamma_{0\parallel} = -\frac{\pi}{2} + \omega_0 T$.
2. The **high-loss regime**. It is located around the output state with a polarization almost perpendicular to the polarization of the input signal, in our case would be the right-handed circular state $|R\rangle$, which entails a Γ around $\Gamma_{0\perp} = \frac{\pi}{2} + \omega_0 T$.

As the name suggests, there are fewer insertion losses in the low-loss regime than in the high-loss regime. Thus, to measure very small delays, the attractive regime will be the one with many losses, and it does not matter if some signal power is lost; what matters is how good a pint-size frequency shift can be measured.

When using WVA to estimate an unknown parameter (a delay introduced T generated by either a Michelson interferometer, the index of refraction Δn of a grating, or even the height d_{step} of a phase object), one has two different measurement options:

- **Option 1: $\Delta\lambda(\Gamma)$ and $L(\Gamma)$ for a fixed T**: Make measurements with many post-selection angles, with the help of a liquid crystal variable retarder, and estimate the unknown parameter making the best fit of the this parameter to the experimental results. In both regimes, some of the relevant data will be: a) the post-selection angle in which $\Delta\lambda(\Gamma_0) = 0$, b) the losses that correspond to that post-selection angle Γ_0 and c) the post-selection angle Γ_{opt} where the maximum wavelength shift $\Delta\lambda_{max}$ can be measured. Thus, in the low-loss regime, one would expect to observe a zero, meaning a Γ at which there are no losses, and very small wavelength shift measurements. On the other hand, in the high-loss regime, one expects more extensive wavelength shift measurements in exchange for maximum losses.

Example 1: Take a delay of $T = 10$, which means that a phase of $\omega_0 T = 1.33^\circ$ is introduced. For the low-loss regime, the zero wavelength shift is obtained at $\Gamma_{0\parallel} = -\pi/2 + \omega_0 T = -88.67^\circ$ (see Figure 2), as the output state, is nearly the same as the input state there are almost no losses. For the high-loss regime, the zero wavelength shift is obtained at $\Gamma_{0\perp} = \pi/2 + \omega_0 T = 91.33^\circ$ (see Figure 3), as the output state is nearly the perpendicular state to the input state, there is a maximum signal loss $L_{max} \sim 65dB$. The maximum wavelength shift is measured using $\Gamma_{opt} \sim 91.33 \pm 0.06^\circ$ around the orthogonal state. Greater wavelength shifts, as high as $\Delta\lambda \sim 6$nm can be observed, most spectrometers

can reach resolutions of up to 0.02 nm, rendering measurable these wavelength shifts. Unfortunately, this measurement is also accompanied by higher losses, more than 60 dB.

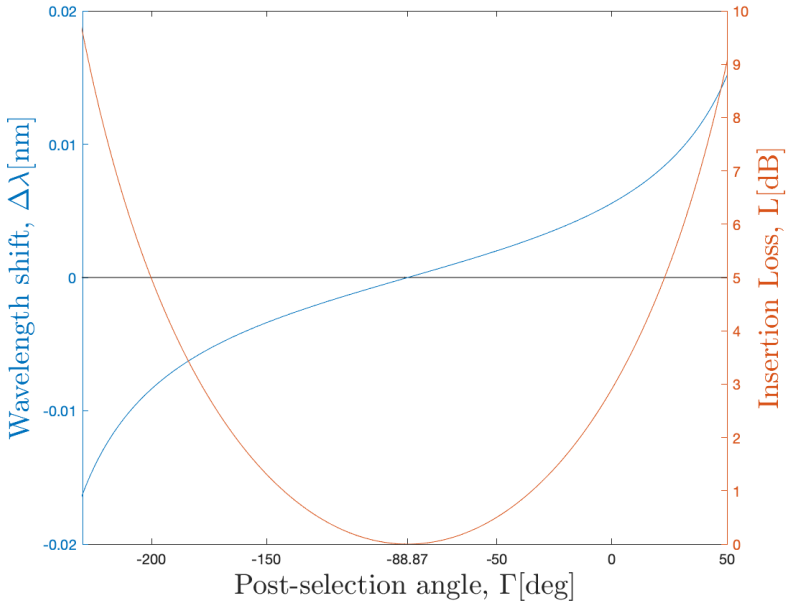

Figure 2. **Example 1A: Centroid of the spectrum and insertion losses VS the post-selection angle in the low-loss regime**. The temporal delay introduced by the Michelson interferometer is $T = 10$as. The low-loss regime includes post-angle selections almost parallel to the polarization of the input signal, that is $|L\rangle$. In blue, the wavelength shift measured in nm and orange the insertion losses in dB, both of them are represented against the post-selection angle Γ. The zero wavelength shift and minimum insertion losses occur for $\Gamma_{0\|} = -88.67°$. Data: $\lambda_0 = 810$nm and $\tau = 11.6$fs.

- **Option 2: $\Delta\lambda(T)$ and $L(T)$ for a fixed Γ_0**: First, a reference delay T_0 is determined, then its post-selection angle $\Gamma_{0\perp}$, where the wavelength shift is zero in the high-loss regime with maximum losses, is chosen. Now the wavelength shifts around this value can be measured to estimate the parameter one has. The data that one wants to extract is a temporal delay T_{opt} responsible for generating a maximum wavelength shift, as well as the range of T where a lineal behavior is observed.

Example 2: We will focus on the same previous example, where the post-selection angle selected is $\Gamma = 91.33°$. The temporal reference delay is fixed at $T_0 = 10$as. In Figure 4, it can be seen that the optimal temporal delays are $T_{opt1} = 9.59$as and $T_{opt2} = 10.45$as. The range of values where the parameter behaves linearly is between those maximums (with absolute value). It can also be observed that the maximum losses are a bit displaced from the reference time delay T_0; the reason is that the parameter $\gamma(T)$ multiplying the cosine in Equation 2.13 depends on T.

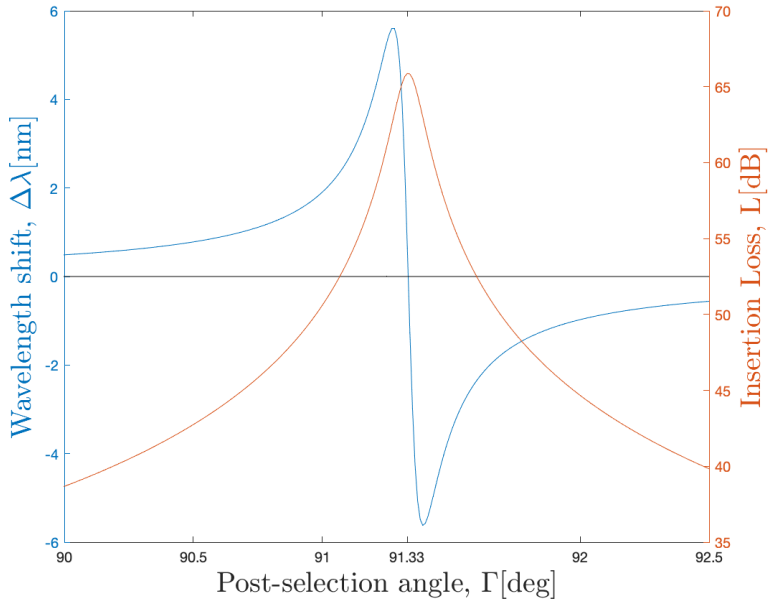

Figure 3. **Example 1B: Centroid of the spectrum and insertion losses VS the post-selection angle in the high-loss regime**. The temporal delay introduced by the Michelson interferometer is $T = 10$as. The low-loss regime includes post-angle selections almost perpendicular to the polarization of the input signal, that is $|R\rangle$. In blue the wavelength shift measured in nm and in orange the insertion losses in dB, both of them represented against the post-selection angle Γ. The zero wavelength shift and maximum insertion losses occur for $\Gamma_{0\perp} = 91.33°$. We reach the maximum value of $\Delta\lambda$ for $\Gamma_{opt} = \Gamma_{0\perp} \pm 0.06°$. Data: $\lambda_0 = 810$nm and $\tau = 11.6$fs.

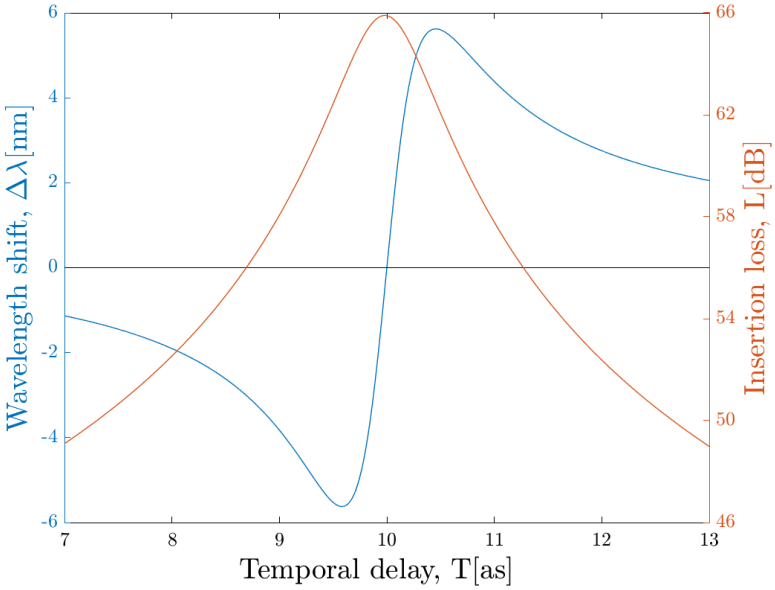

Figure 4. **Example 2: Centroid of the spectrum and insertion losses VS the time delay**. The post-selection angle is fixed at $\Gamma_{0\perp} = 91.33°$ so that when introducing through the Michelson interferometer $T = 10$as, the wavelength shift is zero. In blue, the wavelength shift measured in nm and in orange the insertion losses in dB are both represented against the temporal delay introduced T in as. The optimal temporal delays are $T_{opt1} = 9.59$as and $T_{opt2} = 10.45$as. Data: $\lambda_0 = 810$nm, $\tau = 11.6$ fs and $T_0 = 10$as.

3 Weak Value Amplification for probing sub-wavelength gratings

3.1 Sub-wavelength grating (SWG)

Consider the periodic waveguide structure shown in Figure 5. It consists of a grating made with two homogeneous materials. A refractive index of $\epsilon_1 = n_1^2$ characterizes the core layer and has a thickness of H, a pitch Λ spaced the rectangles at the boundary of two media, the upper cladding with refractive index $\epsilon_2 = n_2^2$ and the substrate with $\epsilon_3 = n_3^2$, but we will take $n_1 = n_3$ from now on for the sake of clarity. It is defined by a filling factor $D = \frac{a}{\Lambda}$, which corresponds to the duty cycle of the structure, and the grating-vector module $K = \frac{2\pi}{\Lambda}$ so that one can express it as a periodic function with a unity pattern formulated as:

$$n_{SWG}^2 = \begin{cases} n_1^2 & \text{for x} \in (0, D\Lambda) \\ n_2^2 & \text{for x} \in (D\Lambda, \Lambda) \end{cases} \tag{3.1}$$

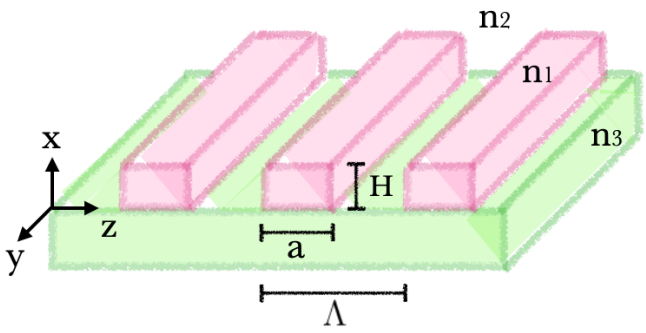

Figure 5. **Grating Schematic**: A 1D Lamellar z-periodic dielectric waveguide structure determined by n_1, n_2, and n_3 is the refractive indexes of the core layer, upper cladding, and substrate materials (typically for simplicity $n_1 = n_3$ and $n_1 > n_2$). It is a crosswise structure as there is a single waveguide array mode propagating along the x-direction.

One must define the Fourier series for further use.

$$n^2(x) = \sum_n a_n e^{iKnx} \text{ where } a_n = \frac{1}{\Lambda}\int dx\, n^2(x) e^{-iKnx} \tag{3.2}$$

and

$$\frac{1}{n^2(x)} = \sum_n b_n e^{iKnx} \text{ where } b_n = \frac{1}{\Lambda}\int dx\, \frac{1}{n^2(x)} e^{-iKnx} \tag{3.3}$$

From the scalar grating equation, the angle of the diffraction orders θ_k is given by $n_d \sin\theta_n = n\frac{\lambda}{\Lambda}$ with $n_d = \max(n_2, n_3)$. Diffraction effects will thus be suppressed for

all orders $|n| \geq 1$ when $|\sin\theta_{\pm 1}| > 1$, that is when $\frac{\lambda}{\Lambda} > n_d$ implying a small pitch, when this happens, this structure can be referred to as a sub-wavelength grating SWG [10],[15]. Therefore this structure only supports a single diffraction order with $n = 0$.

For example, consider the waveguide core made of silicon and both bottom and upper cladding made of silicon oxide, then $n_1 \sim 3,5$, $n_2 \sim 1,45$, and $n_3 \sim 1 - 1,6$. With this data, the results of the sub-wavelength pitches are around the order of $\Lambda \sim 150$nm plus for a free-space wavelength $\lambda \sim 810$nm, one can see that $\Lambda << \lambda$ so that it is the deep-sub-wavelength regime.

For waves propagating perpendicularly to the Lamellar stack, remember that two different electric fields are incising the structure: the parallel (TM polarization) and the perpendicular to the grating vector (TE polarization). Each of them is responsible for the corresponding effective refractive index $n_{\parallel}$ and $n_{\perp}$. The general formulas for an order n are derived in the paper "On the effective medium theory of subwavelength periodic structures" by Lalanne. The expressions are the following (see Eq.(8) and Eq.(17) in [16]):

$$n_{eff\parallel}^2 = a_0 + \left(\frac{\Lambda}{\lambda}\right)^2 \sum_{n\neq 0} \frac{a_n a_{-n}}{n^2} \tag{3.4}$$

$$n_{eff\perp}^2 = \frac{1}{b_0} + \left(\frac{\Lambda}{\lambda}\right)^2 \frac{1}{b_0^3} \sum_{n\neq 0} \frac{b_{-n} \sum_{p\neq 0} \frac{a_{n-p} b_p}{p}}{n} \tag{3.5}$$

For this concrete structure, making use of Equation 3.2, the zero order Fourier coefficients are the following, also known as Ryotov's formula (for a more detailed development, see C):

$$a_0 = D n_1^2 + (1-D) n_2^2; \tag{3.6}$$

$$b_0 = D\frac{1}{n_1^2} + (1-D)\frac{1}{n_2^2}; \tag{3.7}$$

One can substitute the expressions of the n-coefficients into Equation 3.4 and obtains the closed-form EMT solution:

$$n_{eff\parallel}^2 = D n_1^2 + (1-D) n_2^2 + \left(\frac{\Lambda}{\lambda}\right)^2 \frac{(n_1^2 - n_2^2)^2}{\pi^2} \sum_{n\neq 0} \frac{\sin^2(\pi n D)}{n^4} \tag{3.8}$$

$$n_{eff\perp}^2 = \frac{1}{\frac{D}{n_1^2} + \frac{1-D}{n_2^2}} + \frac{\pi^2}{3} D^2 (1-D)^2 \left(\frac{n_1^2 - n_2^2}{n_1^2 n_2^2}\right)^2 \frac{a_0}{b_0^3} \left(\frac{\Lambda}{\lambda}\right)^2 \tag{3.9}$$

Notice that the zero-order in $\frac{\Lambda}{\lambda}$, the static limit, n_{eff}^2 does not depend on the period Λ, just on the duty cycle D, so that we have to work with the first order minimum in order to

be able to retrieve Λ. On the other hand, for a given duty cycle $D \in (0,1)$ and a material with concrete parameters, $\Delta n = n_{\parallel} - n_{\perp} > 0$ always, which means that the dielectric grating is intrinsically birefringence. Also, one should remember that $\lambda\omega = 2\pi c$, so that $\frac{\Lambda}{\lambda} = \frac{\Lambda}{2\pi c}(\omega_0 + \Omega)$ and this means that the effective refractive indexes will depend on the frequency. This relation can be seen in Figure 6. The variation in frequency is very small, almost unnoticed. There can indeed be seen a correction on the static limit, as there is an added term $\neq 0$.

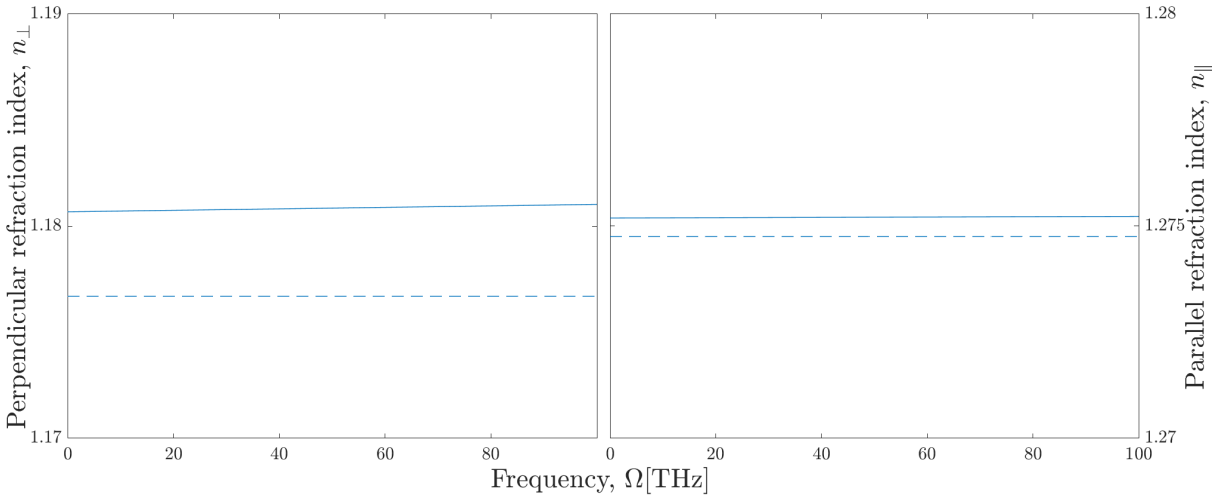

Figure 6. **Perpendicular effective refractive index** (on the left) **and parallel effective refractive index** $n_{\parallel}$ (on the right) **VS frequency**: The dotted lines are for the static order, $n^2_{eff\parallel} = a_0$ and $n^2_{eff\perp} = 1/b_0$ see Equations 3.6 and 3.7. The straight lines correspond to $n(\Omega)$ up to the second order, see Equations 3.8 and 3.9. Data: Duty cyle $D = 0.5$, $n_1 = 1.5$, $n_2 = 1$, period $\Lambda = 150$nm and $\lambda = 810$nm.

The group index does not depend on the frequency, and it is evaluated around the central frequency ω_0:

$$n_g = n(\omega_0) + 2\pi\omega_0 \left[\frac{\partial n(\Omega)}{\Omega}\right]_{\omega_0} = n(\omega_0)\left(1 + \frac{\omega_0\pi}{n^2(\omega_0)}\left[\frac{\partial n^2(\Omega)}{\Omega}\right]_{\omega_0}\right) \tag{3.10}$$

notice that for periods smaller and smaller, we should approach the value valid for the static limit $n_{g,\parallel} \to n_{\parallel}$ and $n_{g,\perp} \to n_{\perp}$.

Therefore the grating generates a delay between horizontal (the parallel component) and vertical (the perpendicular component) polarizations. If a ray of light is sent through the x-axis, the grating adds a different delay in $\widehat{H}$ and $\widehat{V}$ components. The electric field of the beam after passing through the grating will be:

$$E_1 = \frac{E_{in}}{\sqrt{2}}\left(\widehat{H} + i\widehat{V}e^{-i(\omega_0+\Omega)T}\right)e^{i\phi}, \tag{3.11}$$

where the delay introduced reads

$$T = \frac{\Delta n}{c} H = \frac{n_{g,\parallel} - n_{g,\perp}}{c} H \tag{3.12}$$

Furthermore, it can be seen the dependence on the refracting index $T(\Delta n)$, which can be controlled either by changing the duty cycle D, the period Λ of our SWG, or using different materials, which means to monitor the refraction indexes n_1 and n_2.

3.2 Measurement of the temporal delay introduced by the sub-wavelength grating

3.2.1 Example of a sub-wavelength grating

The depth of the grating and the materials are fixed. The chosen value of the depth is $H = 170$nm, very tiny as well as the the pitch at which it is spaced, around $\Lambda = 150$nm (the small values are smartly chosen to introduce the minor realistic time delay with an SWG). As for the refraction index given by the material, imagine using a PMMA grating where both the core layer and substrate material are Poly(methyl methacrylate), and the upper cladding is the air so that in this case, the refractive indexes correspond to $(n_1, n_2, n_3) = (1.5, 1, 1.5)$.

Figure 7 represents Equation 3.12. It shows the time delay in front of both the duty cycle (on the left) for a fixed $\Lambda = 150$nm and the period (on the right) for a fixed $D = 0.5$ when considering the effective refraction indexes up to the second-order (in blue) and in the zero-order also known as the static limit (in orange) where the expressions 3.8 are hugely simplified into $n^2_{eff\parallel} = a_0$ and $n^2_{eff\perp} = 1/b_0$. In both left and right cases, one can observe that the static limit introduces a delay a bit higher. The behavior observed at the left is parabolic, reaching the top value at $T_2 = 52$as in blue and $T_0 = 56$as in orange. At the right is different, one can see that the delay has a constant value of $T_0 = 56$as for the static limit (the effective refractive indexes do not depend on the frequency).

3.2.2 Main results

The goal is to estimate the period Λ of the grating or the duty cycle $D = \frac{a}{a+\lambda}$. For clarity, we will develop just the case where the period is fixed, and the interest variable is the duty cycle plus being in the static limit (the orange curve at the left of Figure 7). We will proceed just as in Section 2.1.3. In the pre-selection stage, one ensures that the polarization of the Gaussian beam is left-handed circular. In the second stage, instead of using a Michelson interferometer, the sub-wavelength grating is used, already analyzed, to introduce the delay seen in Equation 3.12. Finally, in the post-selection, our output state is projected into a state with a polarization determined by Γ, and the wavelength

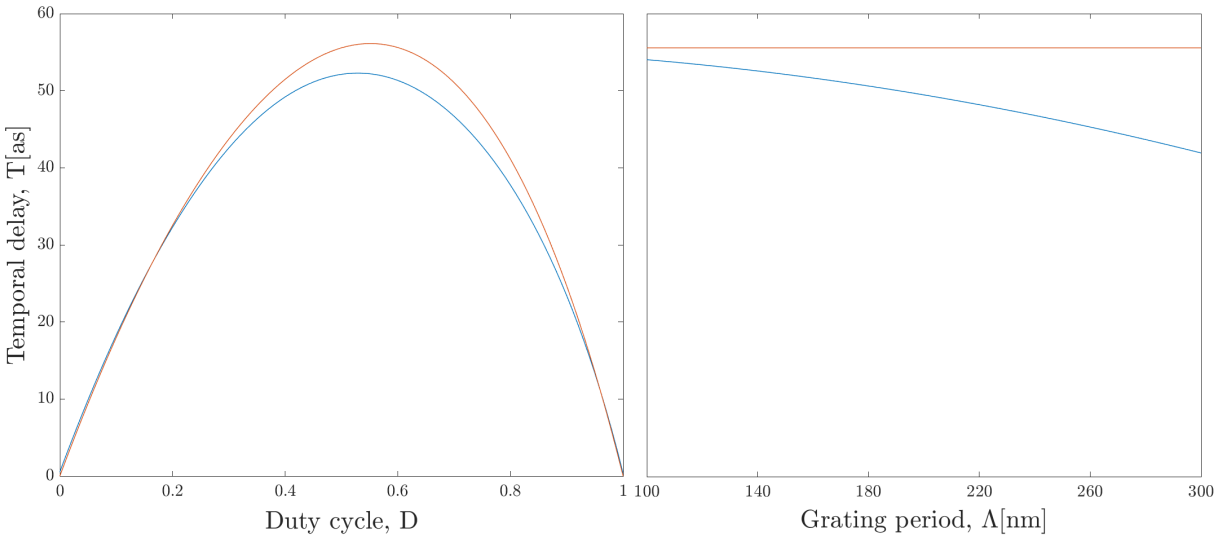

Figure 7. **Temporal delay VS the duty cycle** (left) **/ the grating period** (right). In orange one can see the representation of the static limit, and in blue the refraction index up to the second order. At the left is fixed the period at $\Lambda = 150$nm, and on the right the duty cycle at $D = 0.5$. The temporal delay T is measured in attoseconds. Here is illustrated the relation seen in Equation 3.12. Data: $n_1 = 1.5$, $n_2 = 1$, $H = 170$nm and $\lambda = 810$nm.

shift and insertion losses can be at last represented (using Equations 2.12 and 2.13). Two graphic examples are represented after this, each corresponding to a different option of estimating a parameter using the WVA technique:

Example 1: $\Delta\lambda(\Gamma)$ and $L(\Gamma)$ for a fixed T. In this first example, the grating material is fixed ($n_1 = 1.5$ and $n_2 = 1$), and the duty cycle is variable so that different temporal delays of the order of ~ 50as are introduced. Figure 8 shows the wavelength shift $\Delta\lambda(\Gamma)$ and insertion loss $L(\Gamma)$ sweeping over the post-selection angles around the perpendicular state in the high-loss regime for some values of duty cycle $D \in (0.1, 0.9)$. It can be observed that there are the same curves as in the example shown in Figure 3 but displaced through the x-axis, as the $\Delta\lambda(\Gamma_{0\perp}) = 0$ occurs at a different point $\Gamma_0 = \omega_0 T_i + \frac{\pi}{2}$ depending on the temporal delay introduced. Therefore the maximum losses move as well.

Also, these results can be related to Figure 7. The temporal delay increases for $d \in (0.1, 0.6)$ and then decreases, just as it has been checked. For example, pay attention to the green curve, which corresponds to a duty cycle of 0.5, one can see that $\Gamma_{0\perp} = 97.42°$ and the optimal post-selection angles are $\Gamma_{opt1+} = 97.1°$ and $\Gamma_{opt1-} = 97.9°$.

Example 2: $\Delta\lambda(T)$ and $L(T)$ for a fixed Γ_0: In this second example, both the grating material and the duty cycle are fixed (maintaining the same as before $(n_1, n_2) = (1.5, 1)$ and $D = 0.5$), so that $\Delta n_0 = 0.098$ and the taken reference time delay is $T_0 = 55.5$as (the maximum value for an SWG with n_1 and n_2). The reference angle taken will be the orthogonal $\Gamma_{0\perp} = \omega_0 T_0 + \frac{\pi}{2} = 97.42°$ already seen. With this Γ_0 fixed, one can measure the $\Delta\lambda$ around this fixed value T_0 depending on similar T to estimate the parameter Δn.

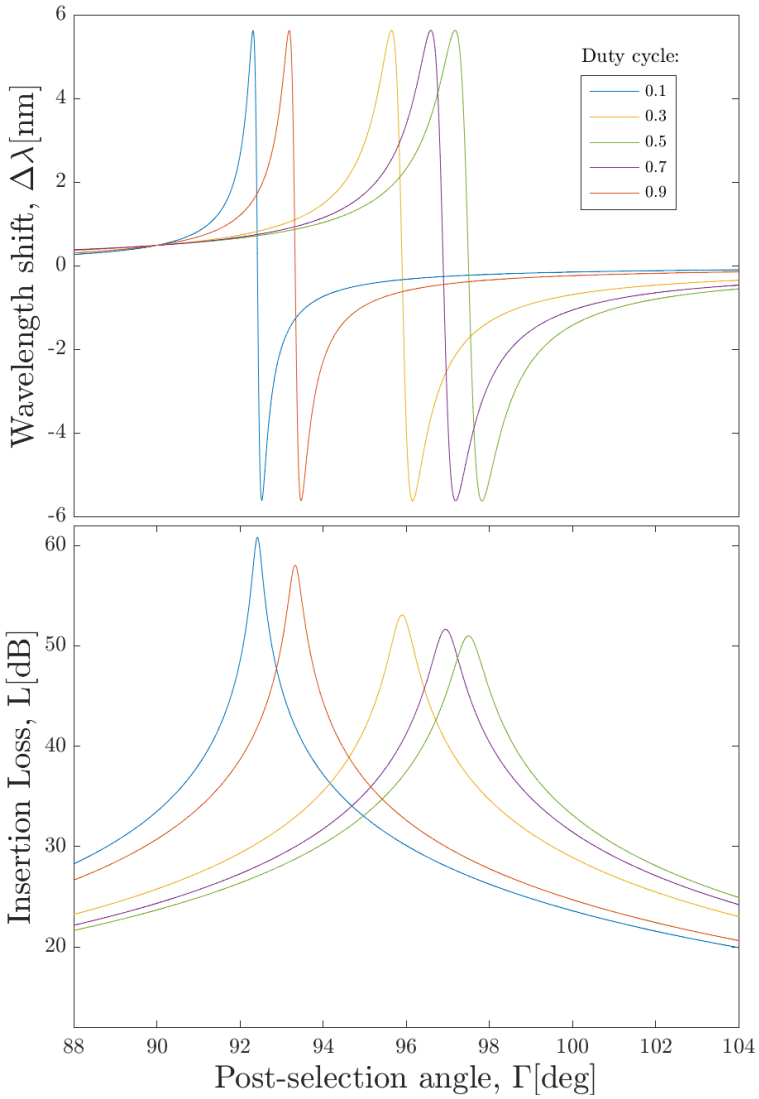

Figure 8. **Example 1: Centroid of the spectrum** (up) **insertion losses** L(down) **VS the post-selection angle for an SWG**. Each color represents a different duty cycle of the sub-wavelength grating, which introduces the corresponding time delay T. For sake of reference, $D = 0.1 \rightarrow T = 17.9$as, $D = 0.3 \rightarrow T = 43.7$as, $D = 0.5 \rightarrow T = 55.6$as, $D = 0.7 \rightarrow T = 51.1$as, and $D = 0.9 \rightarrow T = 24.7$as. Data: $n_1 = 1.5$, $n_2 = 1$, $H = 170$nm, $\lambda_0 = 810$nm and $\tau = 11.6$fs.

In Figure 9 can be observed that there is a linear behavior between $T \in (53.2, 58.1)$as which corresponds to $\Delta n \in (0.094, 0.102) = \Delta n_0 \pm 0.004$. For $n_1 = 1.5$ and $n_2 = 1$, the duty cycle precision is of 0.5 ± 0.066 (notice that the maximum Δn is 0.099).

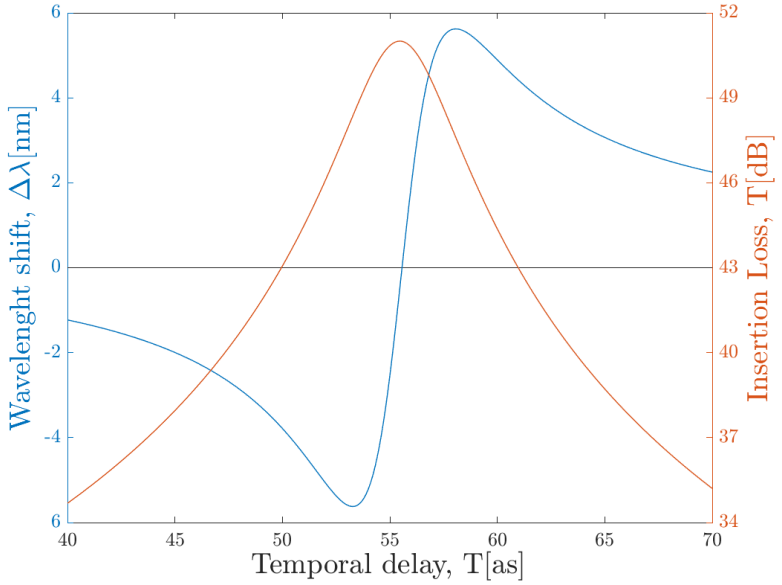

Figure 9. **Example 2: Centroid of the spectrum and insertion losses VS the time delay introduced by the SWG**. The post-selection angle is fixed at $\Gamma_{0\perp} = 97.42°$ so that when introducing through the SWG $T = 10$as, the wavelength shift is zero. In blue, the wavelength shift measured in nm, and in orange, the insertion losses in dB are represented against the temporal delay introduced T in as. The optimal temporal delays are $T_{opt1} = 53.2$as and $T_{opt2} = 58.1$as, and the range of values where the parameter behaves linearly is between both maximums. Data: $\lambda_0 = 810$nm, $\tau = 11.6$ fs and a temporal delay of reference $T_0 = 55.66$as.

4 Weak Value Amplification for imaging edge structures

4.1 Imaging of an edge structure

An edge structure is mainly a phase object. Depicted ideally, phase objects are samples that change the phase but not the light wave amplitude (see Figure 10).

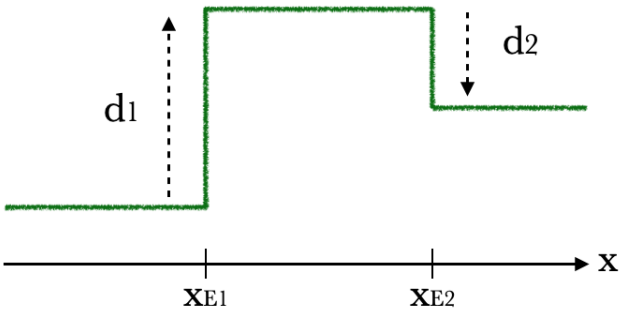

Figure 10. **Example of a phase object**. There is a step that goes up located at x_{E1} of height d_1 and a step that goes down located at x_{E2} of height $-d_2$.

The phase introduced $\phi(x)$ between the horizontal and vertical polarizations correspond to the difference of the paths they travel when bouncing off the phase object, so it will be important the position where the beam is placed:

$$\phi(x) = 2\mathrm{k}d(x) = (\omega_0 + \Omega)\frac{2d(x)}{c}, \tag{4.1}$$

where $d(x) = d_H(x) - d_V(x)$ and the temporal delay is basically $T(x) = 2d(x)/c$. An option to describe the profile of the phase object mathematically is to model its intervention as a sum of step functions multiplied by different phase values:

$$f(x) = \frac{1}{2}\big(1 - \mathrm{sgn}(x - x_{Ei})\big)e^{i\phi} + \frac{1}{2}\big(1 + \mathrm{sgn}(x - x_{Ei})\big) \tag{4.2}$$

$$\phi = (\omega_0 + \Omega)\frac{2d}{c} \tag{4.3}$$

so that at the left of the position x_{Ei} a constant phase ϕ is introduced while at the right there is no phase added and the signal maintains the same.

4.2 Measurement of the temporal delay introduced by the edge structure

Now, the edge structure or phase object introduces a new degree of freedom, space, so it has to be taken into account the spatial Gaussian shape when calculating the output

spectral density. The procedure is very similar to the one developed in Section 2.1.3 (setup seen in Figure 11): A) In the first stage, in blue, a left-handed circularly polarized Gaussian beam $|L\rangle$ is obtained; B) In the second stage, in pink, a time delay that will depend on the position of the beam x_0 is introduced by the phase object; C) Finally, in the third stage, in green, the output state is projected onto $\widehat{e}_{out} = \frac{1}{\sqrt{2}}(\widehat{H} + e^{i\Gamma}\widehat{V})$ so that the wavelength shift and insertion loss can be measured. As the last step, the measures must be repeated while sweeping the beam along the x-axis, retrieving information at each position.

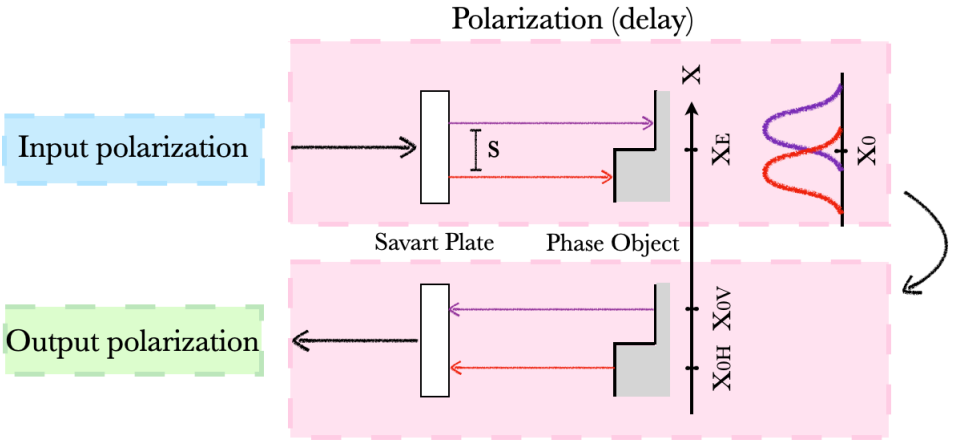

Figure 11. **Setup for introducing a phase with an edged structure**. In pink, the setup for introducing the phase: a Savart plate divides our Gaussian beam centered at x_0 into the horizontal and vertical beams centered correspondingly at x_{0V} and x_{0H}, separated by a distance s; then it shifts the center position again having added a phase ϕ between them. It is clear to see that the delay will depend on the point we direct the laser.

Our input state now will be the following:

$$E_{in}(\Omega, x) = \frac{E_{in}(\Omega)}{\sqrt{2}} \exp\left[-\frac{(x - x_0)^2}{w_{b0}^2}\right](\widehat{H} - i\widehat{V}) \tag{4.4}$$

Aside from the Gaussian frequency shape and left-handed circular polarization, it has to be considered a spatial Gaussian beam with a beam waist w_{0b} centered at x_0. After passing through the Savart plate once, the vertical and horizontal components shifted at $x_0 \pm s/2$. Then it interacts with the phase object, which adds $f(x)$ at each $|H\rangle$ and $|V\rangle$ beams (previously seen in Equation 4.2) and finally, the Savart plate displaces the beams at x_0 again, so that the output electric field depending on the position is:

$$E_{out}(\Omega, x) = \frac{E_{in}(\Omega)}{\sqrt{2}} \exp\left[-\frac{(x - x_0)^2}{\omega_{b0}^2}\right]\left(f(x + s/2)\widehat{H} - if(x - s/2)\widehat{V}\right) \tag{4.5}$$

For a better understanding of the situation, Figure 12 shows the amplitude of the spatial Gaussian beam $A = \frac{E_{in}(\Omega)}{\sqrt{2}} \exp\left[-\frac{(x-x_0)^2}{w_{b0}^2}\right]$ for two different beam waists and the function

$f(x \pm s/2)$ defined for $\phi = \omega_0 T = 180°$. At the right of the step $f(x) = 1$ so that it has no effect when multiplying while at the left we have $e^{i\phi} = -1$. One can see that the narrower the beam waist is, the more difference there will be between the horizontal and vertical components.

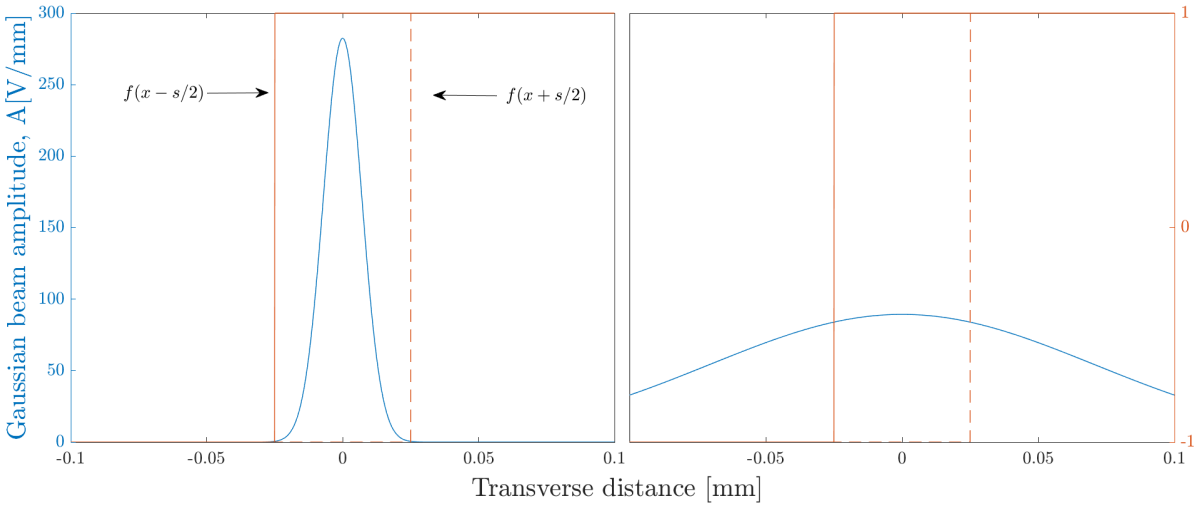

Figure 12. **Gaussian beam amplitude** (in blue) **/ Function displaced** $\pm s/2$ (in orange) **along the transverse distance of an edge structure**. At the left a beam characterized by a beam waist of $w_1 = 10\mu$m and at the right with $w_2 = 100\mu$m. Both are placed at $x_{01} = 0$mm. The dotted line corresponds to $f(x + s/2)$ and the continuous to $f(x - s/2)$, they introduce a phase $e^{i\phi} = -1$ at the left and no change at the right. Data: $d = \lambda/4$, $s = 50\mu$m and $\lambda = 810$nm.

Going on, what interests us is the frequency regime, so that the spatial degree of freedom has to be integrated $E_{out}(\Omega) = \int_{-\infty}^{\infty} dx\, E_{out}(\Omega, x)$, one obtains the following output electric field (see the mathematical development in Appendix B):

$$E_{out}(\Omega) = E_{in}(\Omega)\frac{\omega_{b0}\sqrt{\pi}}{4}\left[\left(1 + e^{-i\phi}\right)\left(1 - ie^{i\Gamma}\right) + \left(1 - e^{-i\phi}\right)\left(\mathrm{erf}_H - ie^{i\Gamma}\mathrm{erf}_V\right)\right] \tag{4.6}$$

Where for the sake of clarity the functions erf_H and erf_V correspond to $\mathrm{erf}\left(\frac{x_{Ei} - x_0 + s/2}{w_{b0}}\right)$ and $\mathrm{erf}\left(\frac{x_{Ei} - x_0 - s/2}{w_{b0}}\right)$, both depending on the position x_0.

Moreover, the output spectral density is written as:

$$S_{out}(\Omega) = S_{0\Omega}\exp\left[-\frac{\tau^2}{4\ln 2}\Omega^2\right]\frac{\omega_{0b}^2\pi}{4}\left(A\sin\phi + B\cos\phi + C\right) \tag{4.7}$$

$$A = \cos\Gamma\left(\mathrm{erf}_H - \mathrm{erf}_V\right) \tag{4.8}$$

$$B = 1 + \sin\Gamma - \frac{1}{2}\left(\mathrm{erf}_H^2 + \mathrm{erf}_V^2 + 2\sin\Gamma\mathrm{erf}_H\mathrm{erf}_V\right) \tag{4.9}$$

$$C = 1 + \sin\Gamma + \frac{1}{2}\left(\mathrm{erf}_H^2 + \mathrm{erf}_V^2 + 2\sin\Gamma\mathrm{erf}_H\mathrm{erf}_V\right), \tag{4.10}$$

notice that the coefficients A, B, and C depend on the positions $x_{0H} = x_0 - s/2$ and $x_{0V} = x_0 + s/2$, on the beam waist w_{b0} and on the post-selection angle Γ. The constant phase ϕ corresponds to Equation 4.3 seen above.

Once the output spectral density has been obtained, the frequency shift and insertion losses can be calculated. Very similar expressions as the ones calculated with the Michelson interferometer are obtained in Equations 4.11 and 4.12 (see the mathematical development in Appendix B). We keep working with the same γ seen in Equation 2.14:

$$\Delta f(\Gamma) = \frac{\ln 2}{\pi}\left(\frac{T}{\tau^2}\right)\frac{\gamma\Big(A(\Gamma)\cos(\omega_0 T) - B(\Gamma)\sin(\omega_0 T)\Big)}{\gamma\Big(A(\Gamma)\sin(\omega_0 T) + B(\Gamma)\cos(\omega_0 T)\Big) + C(\Gamma)} \tag{4.11}$$

$$L(\Gamma) = -10\log\left[\frac{\omega_{0b}^2\pi}{4}\Big(A(\Gamma)\gamma\sin(\omega_0 T) + B(\Gamma)\gamma\cos(\omega_0 T) + C(\Gamma)\Big)\right] \tag{4.12}$$

Analyzing Equation 4.11, one realizes that finding the post-selection angle $\Gamma_{0\perp}$ that describes the orthogonal state $\Delta f(\Gamma_{0\perp}) = 0$ is not that easy as before because in this case, it is the solution to the transcendental equation $A(\Gamma_{0\perp})\cos(\omega_0 T) = B(\Gamma_{0\perp})\sin(\omega_0 T)$.

In order to check if Equations 4.12 and 4.11 behave as expected, Figure 13 shows the coefficients $A(x_0), B(x_0)$ and $C(x_0)$ for $\Gamma_{0\perp} = 90°$, a separation in the Savart plate of $s = 20\mu$m and a beam waist of $w_{0b} = 100\mu$m. It can be checked that far from the step, both A and B are zero so that the frequency shift always reads zero $\Delta f = 0$. On the other hand, at the top of the step, where the maximum delay is introduced $T = \frac{2d}{c}$, $A = 0$, and $B = C$ so that the following expressions are obtained:

$$\Delta f(\pi/2) = -\frac{\ln 2}{\pi}\left(\frac{T}{\tau^2}\right)\frac{\gamma\sin(\omega_0 T)}{\gamma\cos(\omega_0 T) + 1} \tag{4.13}$$

$$L(\pi/2) = -10\log\left[\frac{w_{0b^2}\pi}{4}B\big(\gamma\cos(\omega_0 T) + 1\big)\right] \tag{4.14}$$

Whether or not there is a zero frequency shift at $\Gamma = 90°$ will depend on the phase $\omega_0 T$. Using a step of height $d = \lambda/4$, $\omega_0 T \sim 180°$ and $\sin(\omega_0 T) \sim 0$, so that for the perpendicular post-selection angle, there are zero frequency shift and maximum insertion losses.

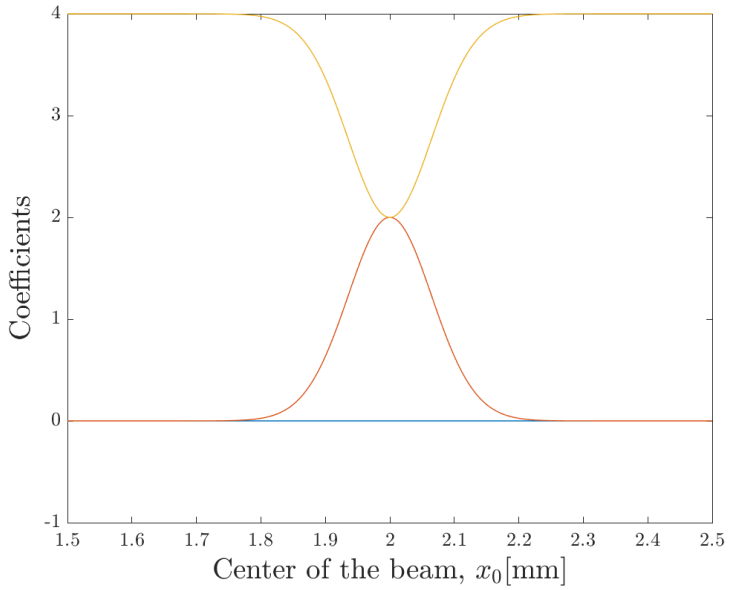

Figure 13. **Coefficients A, B, and C along the x-axis**. In blue A, orange B, and yellow C. For a concrete post-selection angle $\Gamma = 90$ °, each corresponds to these coefficients values when sweeping the beam through a phase object with a step of height d placed at $x_E = 2$ mm. Data: s=20 μm and $w_{0b} = 100$ μm.

4.2.1 Main results

A step of height $d_0 = \frac{\lambda}{4} = 202.5$nm placed in $x = 2$mm is considered. The Savart plate creates an aperture between the beams $\widehat{H}$ and $\widehat{V}$ of $s = 20\mu$m. In order to achieve a better understanding of the results obtained, two different Gaussian beams with their corresponding beam waists will be analyzed: A) $w_{0bA} = 10\mu$m, an ideal case, $w_{0b} << s$ regime; B) $w_{0b2} = 100\mu$m, a much realistic case, $w_{0b} >> s$ regime.

Example 1: $\Delta\lambda(\Gamma)$ and $L(\Gamma)$ for a fixed T. In this first example, the height is d_0, so that a time delay of $T = 2d/c = 1.35$fs is introduced. Figure 14 shows the wavelength shift $\Delta\lambda(\Gamma)$ and insertion loss $L(\Gamma)$ sweeping over the post-selection angles focusing in the high-loss regime for different positions of the beam x_0: starting far from the step (in green) one can see there is no wavelength shift which makes total sense as there is no temporal delay added; when approaching close enough of the step (in orange), one starts observing a wavelength shift; finally, the maximum occurs when being exactly on top $x_0 = x_{E1}$ (in blue), where the measurement reaches almost $\Delta\lambda \sim 6$nm. In all these cases, a significant measure of insertion losses is noted. It can be checked that in both cases w_{0bA} and w_{0bB} the zero wavelength shift and maximum loss occur for $\Gamma_{0\perp} = 90°$. In the ideal case where $w_{0b} << s$ (at the left), there is a narrower variation between the optimal post-selection angles (the linear zone) but higher insertion losses than in the more realistic case, where $w_{0b} >> s$ (at the right). The higher losses are due to the quadratic logarithm relation with the beam waist: $L \propto -10 \log \omega_{0b}^2$.

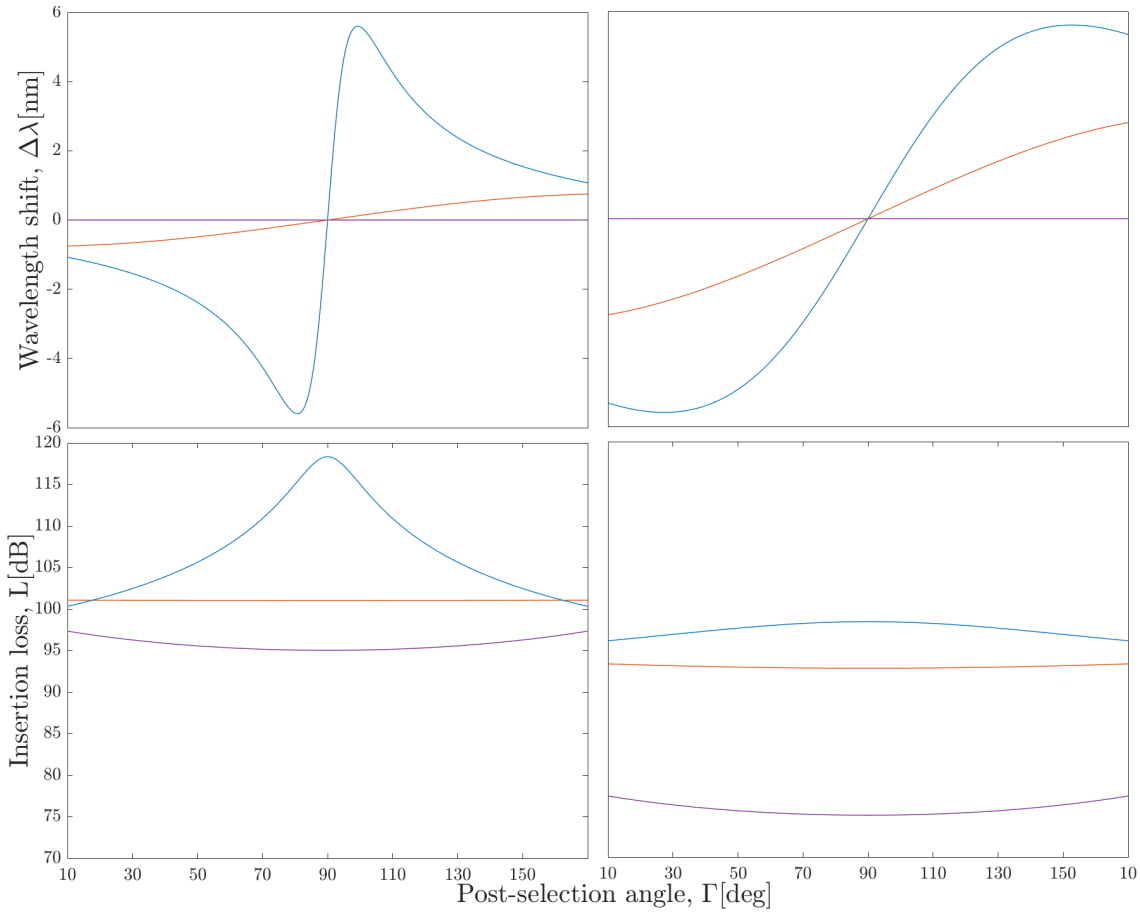

Figure 14. **Example 1A: Centroid of the spectrum** (up) **insertion losses** L(down) **VS the post-selection angle for different positions in an edge structure**. At the left a beam waist $w_{0bA} = 10\mu$m and at the right $w_{0bB} = 100\mu$m. There is a step placed in $x_E = 2$mm of height $d = \lambda/4$. In purple the beam is centered at $x_0 = 1$mm (far from the step), in orange at $x_0 = 1.99$mm (closer to the step) and in blue at $x_0 = 2$mm (on the top of the step). Data: $s = 20\mu$m, $\lambda_0 = 810$nm and $\tau = 11.6$fs.

Take, for example, the curves of the beam at the top of the step, the blue ones where the maximum delay is introduced placed at $x_0 = x_{E1}$. The one at the left (an idealistic case) has the same shape as Figure 3. Let us compare the two cases of beam waists w_{0bA} and w_{0bB}:

	$\Gamma_{opt-}[^\circ]$	$\Gamma_{opt+}[^\circ]$	Lineal range $[^\circ]$	$\Delta\lambda_{max}$[nm]	L_{max}[dB]
w_{0bA}	80.8	99.2	18.4	$\pm$5.6	118.3
w_{0bB}	27.3	152.6	125.3	$\pm$5.6	98.3

Another point of view would be to fix the post-selection angle at $\Gamma_A = \Gamma_{optA+}$ and $\Gamma_B = \Gamma_{optB+}$ correspondingly, and sweep along the phase object (see Figure 15). in Figure 14, at the top of the step, the same results $\Delta\lambda_{max}$ and L_{max} obtained at Γ_{opt+} are observed. The ideal case is better to measure the wavelength shift because the margin of error is ~ 0.01mm, while for w_{0bB} it is more expansive. The displacement seen in the insertion losses is due to the factor previously commented $L \propto -10 \log w_{0b}^2$.

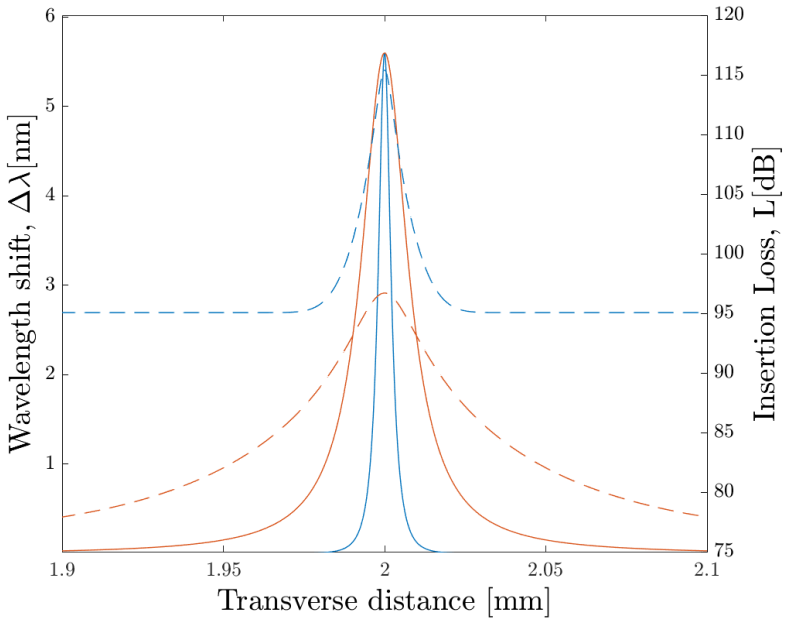

Figure 15. **Example 1B: Centroid of the spectrum** (continuous lines) **insertion losses** (dotted lines) **along the transverse distance of an edge structure**. The blue lines correspond to a beam waist of $w_{0bA} = 10\mu$m and the orange ones to $w_{0bB} = 100\mu$m. Each measures are based on fixing the corresponding positive optimal post-selection angle $\Gamma_{optA+} = 99.2^\circ$ and $\Gamma_{optB+} = 152.6^\circ$. Data: $s = 20\mu$m, $\lambda_0 = 810$nm and $\tau = 11.6$fs.

Example 2: $\Delta\lambda(d)$ and $L(d)$ for a fixed Γ_0. In this second example the height $d_0 = 202.5$nm is fixed so that reference time delay of $T_0 = 2d_0/c = 1.35$fs is introduced. With this data, one can now take the reference angle as the corresponding post-selection angle responsible for detecting a zero wavelength shift already seen $\Gamma_0 = 90^\circ$. With this Γ_0 fixed, one can measure the $\Delta\lambda$ along with the parameter d around the fixed value d_0.

In Figure 16 can be seen that the wavelength shift curve is the same for both w_{0b} and that one still has higher losses for the narrower beam waist w_{0bA}. Also, for $d > 202.5$nm, $\Delta\lambda > 0$ while for $d < 202.5$nm, $\Delta\lambda < 0$. A linear range $\in (194, 211.7)$nm can obtain a good measure for $d = d_0 \sim \pm 9$nm.

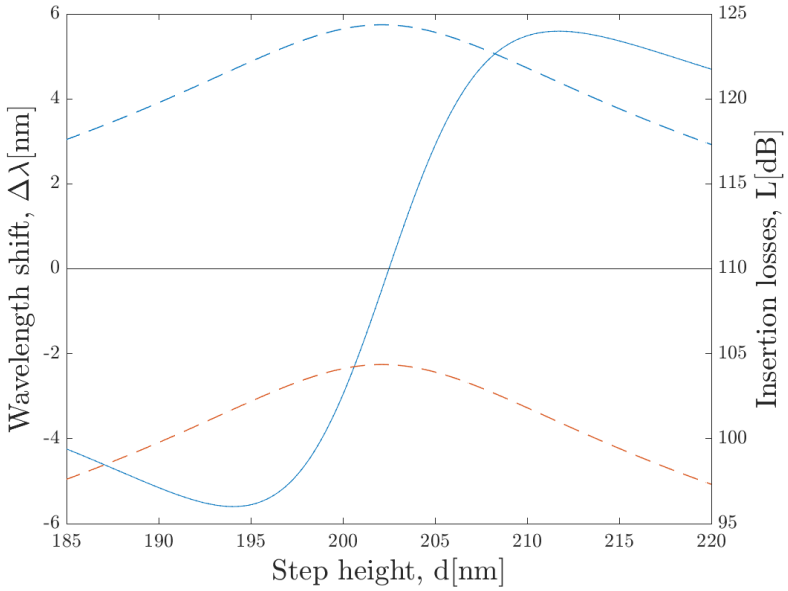

Figure 16. **Example 2A: Centroid of the spectrum** (continuous lines) / **insertion losses** (dotted lines) **VS the height of the edge structure**. Blue lines correspond to $w_{0b1} = 10\mu$m and orange ones to $w_{0b2} = 100\mu$m. Each measures are based on fixing post-selection angle accountable for a zero wavelength shift at $d_0 = \lambda/4$, which is $\Gamma_0 = 270°$. Data: $s = 20\mu$m, $\lambda_0 = 810$nm and $\tau = 11.6$fs.

This second option where the independent variable of the measures is the parameter d with a fixed post-selection angle can be advantageous when detecting manufacturing errors in the step of a phase object of, for example, a height $d_0 = 202.5\text{nm} = \lambda/4$ introducing a phase of $\phi = 4\pi d/\lambda = \pi$ theoretically. When sweeping along the phase object and obtaining the wavelength shift for each point, it is known that any non-zero measure will correspond to a different height d than d_0, this information along with Figure 16 (the one containing the results of using the second option as a measurement method), help us relate this new measures of both $\Delta\lambda(d)$ and $L(d)$ with the actual value of the step height and therefore the phase ϕ it is introducing.

Finally, the last approach one can think of is detecting an error in the value of a known parameter. Figure 17 shows four examples of two steps placed at $x_{E1} = 2$mm and $x_{E2} = 4$mm, where both have a supposed height of $d = d_0$. However, each has a different manufacturing error so that $d \sim d_0$: a) the first one truly has a height of d_0 so that the measure of wavelength shift is zero, while the other one has a measure of about $\Delta\lambda \sim 2$nm, checking with Figure 16, it corresponds to $d = 204.2$ so that it is introducing a phase of 1.0084π instead of $\phi = \pi$; b) the resolution limit occurs for steps of $d =$

$d_0 \pm 0.8\text{nm} d_0(0.25 \pm 0.001)$, where the measurement reaches almost $|\Delta\lambda| \sim 1\text{nm}$; c) in this case one has two d that generate the same measure of wavelength shift, now it is interesting to take a look on the insertion loss, as they will determine the corresponding d value; and d) two d that generate the same value measured of wavelength shift but can be distinguished because of the opposite signs.

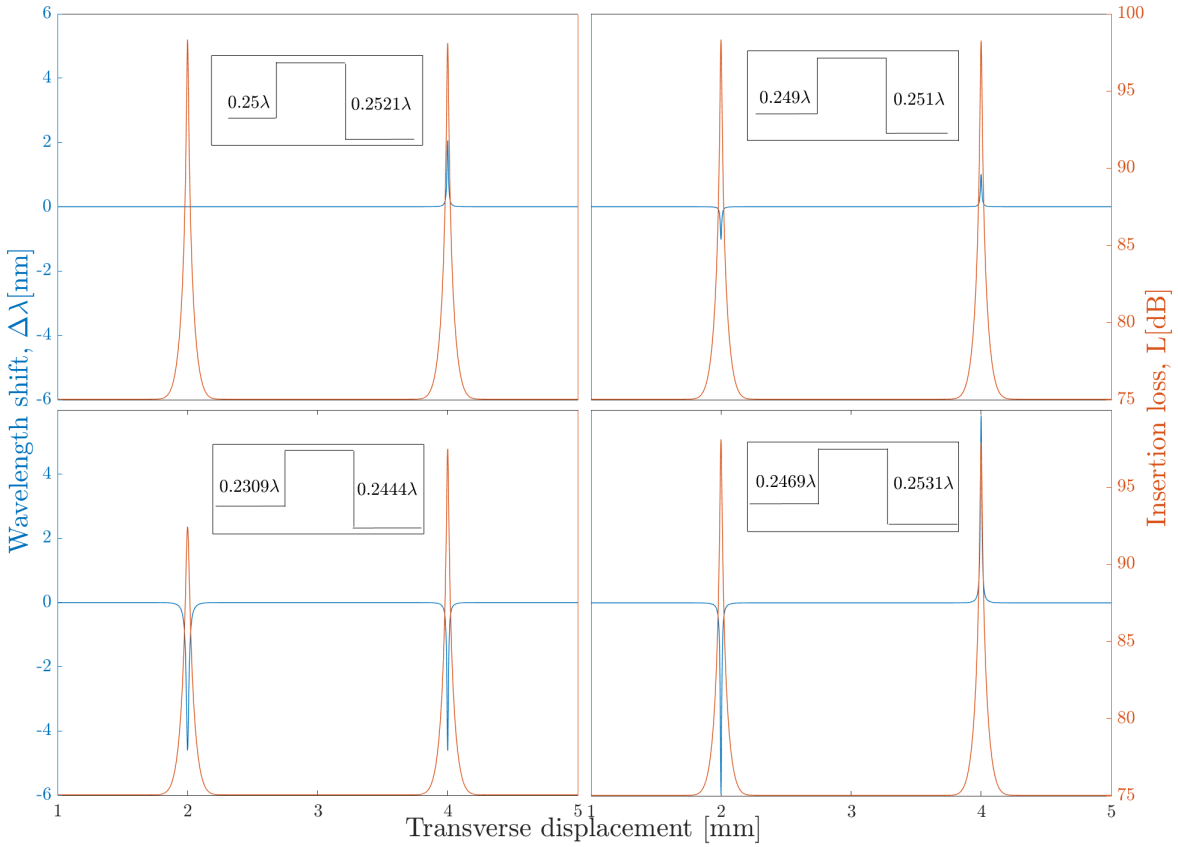

Figure 17. **Example 2B: Centroid of the spectrum** (in blue) **/ insertion losses** (in orange) **along the transverse distance on an edge structure**. Measures taken with a fixed $\Gamma_0 = 90°$, for a reference parameter $d_0 = \lambda/4$. Four different cases with 2 steps placed at $x_{E1} = 2\text{mm}$ and $x_{E2} = 4\text{mm}$ with heights slightly altered than d_0. Data: $w_{0b2} = 100\mu\text{s}$, $s = 20\mu\text{m}$, $\lambda_0 = 810\text{nm}$ and $\tau = 11.6\text{fs}$.

5 Hong-Ou-mandel effect for imaging

5.1 What is the Hong-Ou-mandel effect (HOM)

The Hong-Ou-mandel effect is a two-photon interference effect in quantum optics demonstrated in 1987 by three physicists from the University of Rochester: Chung Ki Hong, Zheyu Ou, and Leonard Mandel [7].

Take into consideration the following setup in Figure 18: two input signals a_1 and a_2 that go through an ideal beam splitter and become two output states a_3 and a_4 measured with independent detectors D_1 and D_2. Therefore, an input photon can take two paths, up and down and the correspondent detector will "click" when it finds the photon.

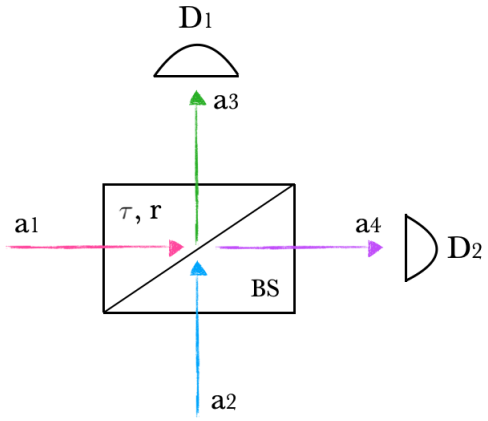

Figure 18. **Beam splitter configuration**. Input signals: a_1 and a_2. Beam splitter characterized by its reflection and transmission coefficients r and τ. Output signals: a_3 and a_4. Two detectors D_1 and D_2.

The Hong-Ou-mandel effect states that if the input signals are identical in their physical properties (polarization, spatio-temporal mode structure, and frequency), meaning that the two states are indistinguishable, there will be no coincidences between the two detectors (they will not "click" at the same time) since the two photons will always exit the beam splitter together in the same output mode (with a 50:50 chance of exiting either one). Therefore, this effect is based on the measurement of correlations and phase intensity, rather than the measurement of the delay introduced as we previously did with Weak Value Amplification.

- Physical description:

When a photon enters a beam splitter it will either be reflected or transmitted so technically there are four possibilities for the photons to behave at the amplitude level. Represented in Figure 19.

On the other hand, the quantum evolution of the beam splitter requires reversibility (being unitary), and this property is achieved be introducing a relative phase shift of π

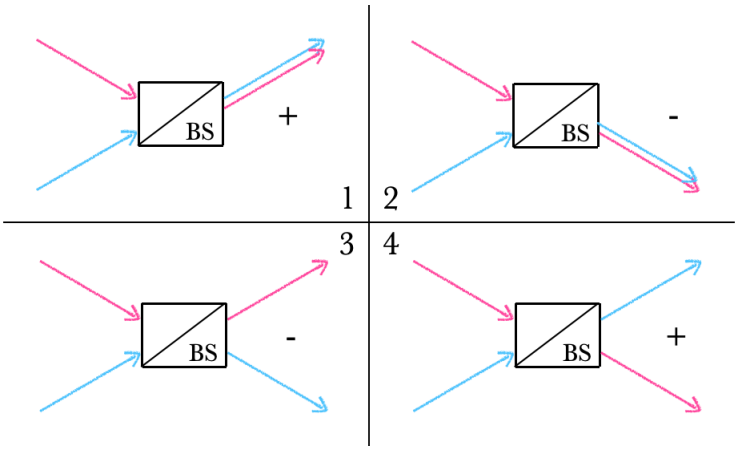

Figure 19. **Possibilities of the behaviour of the photons when crossing the beam splitter**. 1) The photon coming in from above is reflected and the photon coming in from below is transmitted. 2) The photon coming in from above is transmitted and the photon coming in from below is reflected. 3) Both photons are reflected. 4) Both photons are transmitted. The $\pm$ sign correspond to their positive or negative contribution to the superposition.

in the reflection from the bottom side of the beam splitter, corresponding to a factor of -1 in the associated term in the superposition. This leads us to conclude than when accounting the detection of coincidences (possibilities 1 and 2), if the states are equal, their relative minus sign ensures that these two terms cancel. This is why, if they become more distinguishable, the probability of them going to different detectors will increase.

- Mathematical description:

For sake of incoming computations this description of the effect is necessary. Since this effect relies on the existence of photons it can not be fully explained by classical optics, this is why the notation used in this section will be the *bra-ket* (effectively established in 1939 by Paul Dirac [17]).

To do a very simplified and clarifying example, let us only consider states characterized by polarization, regardless of the frequency or the position. Imagine an input state containing two identical input signals, for example, both signals diagonally polarized $|D\rangle$. The input signal will be expressed using creation operators $a_D^\dagger$ over the initial state $|0\rangle$, which increases the number of particles in the given state by one: $|\Psi_{in}\rangle = |\Psi_1\rangle\,|\Psi_2\rangle = a_D^\dagger a_D^\dagger\,|0\rangle = |11\rangle$. Then this signal goes through the beam splitter (BS) and suffers the transformations $a_1^\dagger \to r^* a_3^\dagger + \tau^* a_4^\dagger$ and $a_2^\dagger \to \tau^* a_3^\dagger + r^* a_4^\dagger$:

$$|\Psi_{out}\rangle = r^*\tau^*\big((a_3^\dagger)^2 + (a_4^\dagger)^2\big)\,|0\rangle + a_3^\dagger a_4^\dagger\big((r^*)^2 + (\tau^*)^2\big)\,|0\rangle \tag{5.1}$$

Any beam splitter is characterized by its reflection coefficient r and transmission coefficient τ. When considering an ideal one, both coefficients have to fulfil the following condition:

$$r = Re^{i\alpha} \tag{5.2}$$

$$\tau = \sqrt{1-R^2}\, e^{i(\frac{\pi}{2}-\alpha)} \tag{5.3}$$

For simplicity, the R and α parameters that characterize it will be $R = 1/\sqrt{2}$ and $\alpha = 0$, such that the coefficients become $r = 1/\sqrt{2}$ and $\tau = i/\sqrt{2}$. So that the output state reads:

$$|\Psi_{out}\rangle = -\frac{i}{2}\big((a_3^\dagger)^2 + (a_4^\dagger)^2\big)\,|0\rangle = -\frac{i}{2}(|20\rangle + |02\rangle), \tag{5.4}$$

being $|20\rangle$ and $|02\rangle$ the state where two photons are detected at D_1 and D_2 correspondingly. Therefore, the probabilities of detecting any signal in D_1 (P_{D1}), in D_2 (P_{D2}), or in both at the same time ($P_{D1,D2}$) can now be easily calculated:

$$P_{D1} = P_{D2} = \big|\,\langle\Psi_{20}|\Psi_{out}\rangle\,\big|^2 = \left|\frac{-i}{\sqrt{2}}\right|^2 = \frac{1}{4} \tag{5.5}$$

$$P_{D1,D2} = \big|\,\langle\Psi_{11}|\Psi_{out}\rangle\,\big|^2 = 0 \tag{5.6}$$

One obtains, as expected that the probability of having any coincidence when starting with two identical signals is $P_{D1,D2} = 0$. Notice that the states suffering transformations have not been normalized.

Finally, the Hong–Ou–Mandel effect can be used to test the degree of indistinguishability of two incoming photons. In 2002, it was used to demonstrate the purity of a solid-state single-photon source by feeding two successive photons from the source into a 1:1 beam splitter [18].

5.2 Quantum Differential Interference Contrast (QDIC)

The Differential Interference Contrast (DIC) works on the principle of interferometry to gain information about the optical path length of the sample. Interferometers are based on splitting into two beams the light from a single source. These two travel in different optical paths and then are combined again to produce interference. The resulting interference fringes give information about the difference in optical path lengths so that one measures phase shifts $\Delta\phi$. The technique was developed by Polish physicist Georges Nomarski in 1952 [9].

It becomes a "quantum-DIC" because in order to retrieve information we make use of the Hong-Ou-mandel effect, so that the quantum concept is introduced (see the proposed experiment where the local amplitude and phase of a photon are retrieved using QDIC

[19]). On the other hand, it is essential to work with separable states. If we work in the frequency regime, just as we did in the previously seen WVA technique, it is very challenging to obtain separable states because it is complicated to implement them in the laboratory. That is why we move on to the space regime from now on.

The experimental configuration will be the one seen in Figure 20. Two different light sources will be used, and each of them will go through a sample that will create a DIC. One of them will be introducing a phase ϕ currently unknown, and the other one (an SLM) a phase β that is under our control. These two beams will then be combined in the beam splitter, and finally, the detections measured will be used to reach a conclusion based on the Hong-Ou-mandel effect. We need two single-photons because the HOM can not detect a global phase and we will use the phase added by the phase object as a measurement of polarization in regard to the other beam.

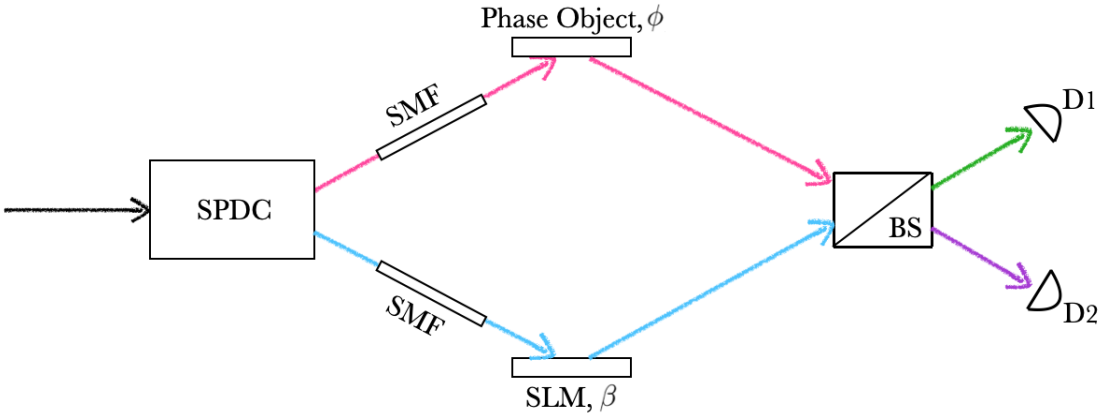

Figure 20. **Setup of the QDIC** (retrieving a phase introduced using HOM). Describing the items sweeping from left to right: In black, the photons entering; SPDC (spontaneous parametric down-conversion) converts the input pump photon into a pair of photons; In pink, the signal photon $|\Psi_s\rangle$ and in blue the idler photon $|\Psi_i\rangle$, of lower energy but with the same polarization; Two SMF (single-mode fiber) to ensure a single-mode, pure and not entangled, in each path; Up/down a phase ϕ/β introduced by either an SWG or a phase object/an SLM (spatial light modulator, able to create a patron $\beta(x, y)$); A beam splitter, in green and purple the output signals detected by the detectors D_1 and D_2.

Remember that the HOM is clear that when there is a detection of zero coincidences, it means that the two input states are the same, and therefore they have suffered the same phase addition resulting in the same polarized state. Therefore, this null detection of coincidences will provide us with the value of phase introduced in the SLM that is the same as the phase introduced by either the SWG or the edged structure. Finally, one can easily retrieve the given unknown parameter (duty cycle D, refractive index Δn or height of the object d).

The experiment aims to obtain the probability of coincidence depending on the selected angle in the SLM $P_{cc}(\beta)$, which can be non-dependant on the space like using a grating

or space-dependent like when using an edged structure. In order to do it, the analytical expression of the output state after passing through the beam splitter must be obtained. First of all, the input state reads $|\Psi_{in}\rangle = |\Psi_s\rangle\,|\Psi_i\rangle$. In order to be as general as possible, our signal (in pink) and idler (in blue) states will be described as follows:

$$|\Psi_s\rangle = \frac{1}{\sqrt{2}}\int dx\big[f_H(x)a^\dagger_{H1}(x) + f_V(x)a^\dagger_{V1}(x)\big]\,|0\rangle \tag{5.7}$$

$$|\Psi_i\rangle = \frac{1}{\sqrt{2}}\int dx\big[g_H(x)a^\dagger_{H1}(x) + g_V(x)a^\dagger_{V1}(x)\big]\,|0\rangle \tag{5.8}$$

where all the functions $f_H(x), f_V(x), g_H(x)$ and $g_V(x)$ are considered normalized. Notice that the only difference between $f_i(x)$ and $g_i(x)$ will be the phase added. The one in the signal state will correspond to the specific phase introduced by either the SWG or the phase object, while the one in the idler state will be phase-controlled for us to be modified as we see fit.

At the next stage, once it has passed through the beam splitter and the corresponding transformations have been applied, the output state obtained is $|\Psi_{out}\rangle = |\Psi_{s2}\rangle\,|\Psi_{i2}\rangle$, where

$$|\Psi_{s2}\rangle = \frac{1}{\sqrt{2}}\int dx\big[f_H(x)r^*a^\dagger_{H3}(x) + f_H(x)\tau^*a^\dagger_{H4}(x) + f_V(x)r^*a^\dagger_{V3}(x) + f_V(x)\tau^*a^\dagger_{V4}(x)\big]\,|0\rangle \tag{5.9}$$

$$|\Psi_{i2}\rangle = \frac{1}{\sqrt{2}}\int dx\big[g_H(x)\tau^*a^\dagger_{H3}(x) + g_H(x)r^*a^\dagger_{H4}(x) + g_V(x)\tau^*a^\dagger_{V3}(x) + g_V(x)r^*a^\dagger_{V4}(x)\big]\,|0\rangle \tag{5.10}$$

Now what interests us is the sum of probabilities of detecting each possible state of coincidences, which are those states where either a $|H\rangle$ or $|V\rangle$ are detected in both detectors 3 and 4: $|\Psi_{cc}\rangle \in (a^\dagger_{H3}(x)a^\dagger_{H4}(x)\,|0\rangle\,,\ a^\dagger_{H3}(x)a^\dagger_{V4}(x)\,|0\rangle\,,\ a^\dagger_{V3}(x)a^\dagger_{H4}(x)\,|0\rangle\,,\ a^\dagger_{V3}(x)a^\dagger_{V4}(x)\,|0\rangle)$, which can be rewritten as $|\Psi_{cc}\rangle \in (|H,H\rangle\,,|V,H\rangle\,,|H,V\rangle\,,|V,V\rangle)$ On the other hand, this probability can be calculated as $P_{cc} = |\,\langle\Psi_{out}|\Psi_{cc}\rangle\,|^2$. Notice that it is not normalized, as it will be important the number of losses obtained. The probability of coincidence will be the following (see Appendix D to see all the development):

$$P_{cc} = \frac{1}{2} - \frac{1}{8}|\rho_H + \rho_V|^2,\ \ \rho_i = \int dx f_i(x)g_i^*(x) \tag{5.11}$$

where ρ_i is essentially the overlap between the states of the component i. ρ will be in the range of values $\in (0,1)$, 1 for when they are the same state and 0 for the case where they are entirely orthogonal.

5.3 For probing sub-wavelength gratings

In this section we intend to apply this method to retrieve a phase introduced by a sub-wavelength grating. Notice that it will be valid for any phase object introducing a delay so that $\phi = \omega_0 T$. A normalized spatial Gaussian beam of a bandwidth ω centered at x_0 defined as

$$\Psi_0(x) = \left(\frac{2}{\pi\omega^2}\right)^{1/4} \exp\left[-\frac{(x-x_0)^2}{\omega^2}\right], \tag{5.12}$$

is considered. After going through the SWG, there will be a phase ϕ and β at each branch, so that the signal and idler states read:

$$|\Psi_s\rangle = \frac{1}{\sqrt{2}} \int dx \left[\Psi_0(x) a^\dagger_{H1}(x) + \Psi_0(x) e^{i\phi} a^\dagger_{V1}(x)\right] |0\rangle \tag{5.13}$$

$$|\Psi_i\rangle = \frac{1}{\sqrt{2}} \int dx \left[\Psi_0(x) a^\dagger_{H1}(x) + \Psi_0(x) e^{i\beta} a^\dagger_{V1}(x)\right] |0\rangle \tag{5.14}$$

where it can be easily identified $f_H(x) = \Psi_0(x)$, $g_H(x) = \Psi_0(x)$, $f_V(x) = \Psi_0(x)e^{i\phi}$ and $g_V(x) = \Psi_0(x)e^{i\beta}$. Therefore, the overlap in the horizontal and vertical components will be $\rho_H = \int dx f_H(x) g^*_H(x) = 1$ and $\rho_V(\beta) = \int dx f_V(x) g^*_V(x,\beta) = e^{i(\phi-\beta)}$. Applying Equation 5.11, one obtains a probability of:

$$P_{cc}(\beta) = \frac{1}{2} - \frac{1}{8}|1 + e^{i(\phi-\beta)}|^2 = \frac{1}{4}\left|e^{i\beta} - e^{i\phi}\right|^2 \tag{5.15}$$

- Numerical example

Taking the previous example used, $(D, n_1, n_2) = (0.5, 1.5, 1)$ with a height of $H = 170$nm, the delay introduced is $T_0 = \frac{n_\parallel - n_\perp}{c} H = 0.05566$fs and therefore, the added phase is $\phi_0 = \omega_0 T = 7.42°$. Figure 21 shows a null probability of coincidence when fixing β at this concrete phase ϕ_0 introduced by the SWG, meaning that both input and output states are identical. With this method, one can retrieve ϕ_0 and, therefore, the correspondent temporal delay T_0, revealing an unknown parameter, either the duty cycle D or the refractive index Δn. It can be seen that expecting a maximum probability of 0.1 to consider a shallow result, the phase extracted can be in a wide range $\phi \in (-38.28°, 53.54°)$, $\Delta\phi \sim 91.8°$ so a not very good precision is achieved with this method.

5.4 For imaging edge structures

In this section we intend to apply the QDIC to retrieve a phase introduced by an edge structure. Notice that this development is valid for any object introducing a phase $\phi(x)$ depending on the space. Therefore, one expects to be able to retrieve the unknown profile introduced in between the horizontal and vertical components.

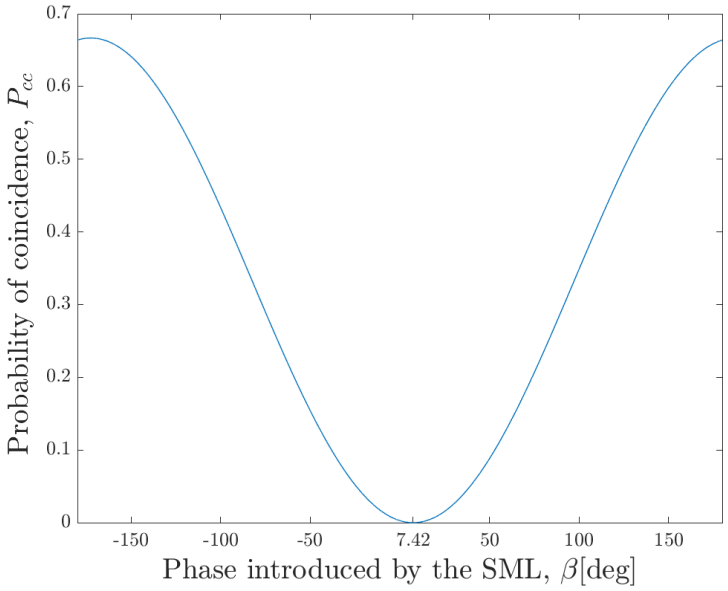

Figure 21. **Probability of coincidence VS the phase introduced by the SLM**. Representation of Equation 5.15. Data: $\beta \in (-180°, 180°)$ and $\phi = 7.42°$.

For sake of feasibility we will consider to different structures:

– A tilted step with an inclination of Φ and height d placed at x_E:

$$\phi_1(x) = kd(1 - \tanh(\alpha(x - x_E))), \quad \text{where } \alpha = \frac{2\tan\Phi}{d} \tag{5.16}$$

– A concave mirror of dimension a:

$$\phi_2(x) = 2\pi\left(\frac{x}{a}\right)^2 \tag{5.17}$$

The procedure starts with identifying the signal and idler states in the same form as Equation 5.8. The probability expression $P_{cc}(x, \beta)$ previously obtained in Equation 5.11 can be applied. Both the horizontal and vertical overlaps ρ_H and ρ_V must be calculated numerically for each pixel, evaluating the integral along with small intervals of space. The aim is to identify the angle where a minimum is detected at each of these pixels so that the spatial phase map needed in the $\beta(x)$ can be recreated point by point. Notice that the overall probability of coincidence P_{cc} will read zero when applying that concrete $\beta(x)$.

In order to develop this method, we consider a spatial Gaussian beam at both components and a difference between them of a phase $\phi_1(x)$ or $\phi_2(x)$. So that we have $f_H(x) = \Psi_0(x)$, $g_H(x) = \Psi_0(x)$, $f_V(x) = \Psi_0(x)e^{i\phi_i(x)}$ and $g_V(x) = \Psi_0(x)e^{i\beta(x)}$. Therefore, the overlap in the horizontal and vertical components will be $\rho_H = \int dx f_H(x)g_H^*(x) = 1$ and $\rho_V(\beta) = \int dx f_V(x)g_V^*(x, \beta) = \int dx|\Psi_0(x)|^2 e^{i(\phi(x)-\beta(x))}$.

When doing simulations, one realizes that a critical constraining parameter is the width of the pixel. Also, the probabilities when evaluating microscopic sections never arrive at zero; the overall zero probability should be obtained when considering the hole. In Figure 22 we can observe the phase retrieved at each point of the SLM for both tilted step and concave mirror. The resolution of the pixel has been amplified we now present a separation of 1 Micra between points.

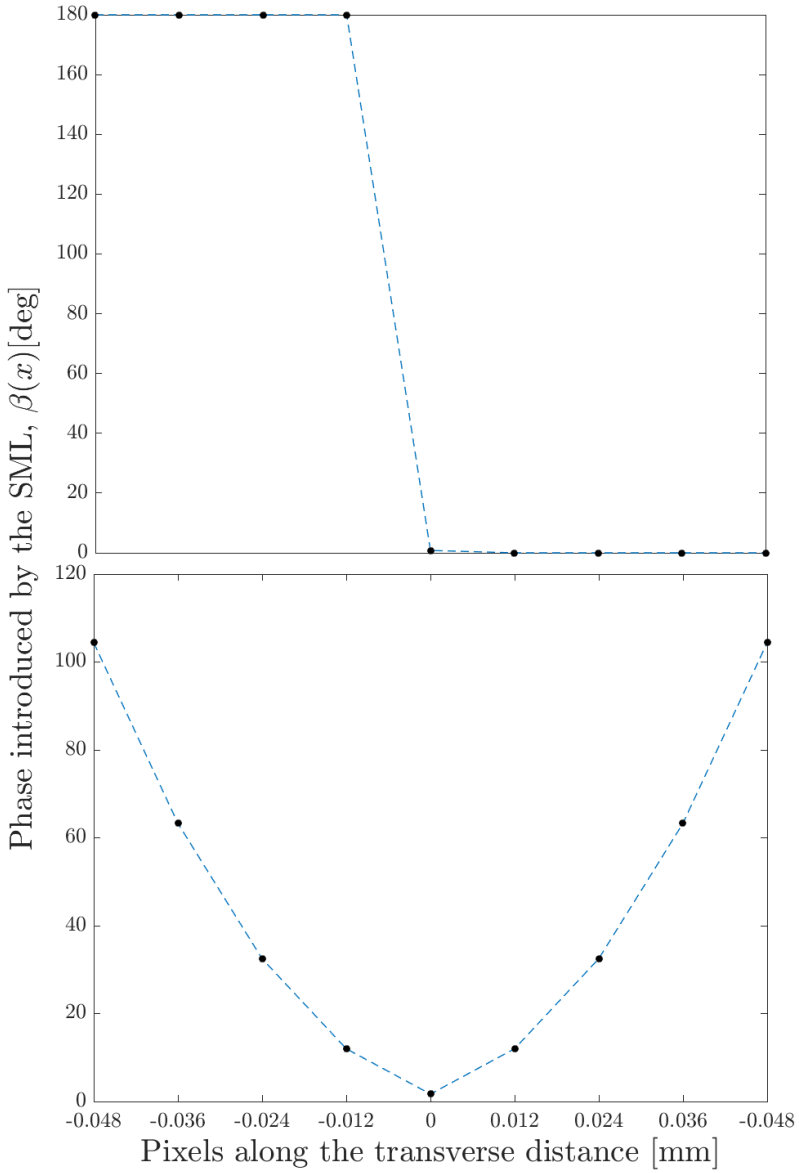

Figure 22. **Phase introduced by the SLM along the transverse distance**. The circles represent the phase retrieved at each pixel. Upward, a phase simulating a tilted step (Eq. 5.16). Downward, a phase with a quadratic behaviour simulating the effect introduced by a concave mirror (Eq. 5.17). Data: $\omega = 100\mu$m, $x_0 = 0$, $d = \lambda/4$, $\Phi = 40\,$deg, $s = 50\mu$m and $\lambda = 810$nm.

6 Conclusions

In this project we have thoroughly analyzed two techniques, Weak Value Amplification and Quantum Differential Interference Contrast. They allow us to measure extremely small delays, reaching the order of attoseconds, and this allows to estimate concrete parameters of relevant phase objects considered.

The two most relevant expressions of the WVA technique have been derived (the frequency shift and insertion losses, see in Eq. 2.12 and 2.13), and it has been seen that we have several ways of reading the information it provides us. On the one hand, we can make measurements with many post-selection angles and estimate the unknown parameter making the best fit of the parameter to the experimental results. On the other hand, we can also set a specific reference parameter and analyze the behavior around this value. In this way, we can detect manufacturing errors.

Three different scenarios have been considered. In all three, the technique offers a maximum wavelength shift of ± 6 nm. These results are entirely satisfactory since the state of art of standard measures allows measuring 0.1nm frequency shifts. First, we have worked with the Michelson interferometer, which has allowed us to introduce delays as small as 10as and has served as a very clarifying example (already exposed in [6]). Secondly, we have worked with sub-wavelength gratings and their effective refractive index from the static limit to the second order. As a result, the duty cycle could be retrieved with an introduced delay of 50as. Finally, a setup has been proposed to obtain the profile of an edge structure. In the latter case, the variable of interest is the height of a step of around 200 nm, so the delay introduced is a bit higher, around 1.3fs.

The other part of the project, which is the quantum sensing through the Hong-Ou-Mandel effect, has been successful. The setup proposed for the QDIC has allowed us to find the value of the specific parameter of interest and recover the spatial profile of an edge structure, such as a step or a concave mirror, by finding the minimum probability of detecting coincidences given by equation 5.11.

To sum up, WVA can be used to detecting SWG and imaging edged samples, and the QDIC can effectively carry out phase retrieval.

For further work, all these techniques and configurations theoretically proposed could be carried out experimentally in the laboratory. In particular, the research group "Quantum Engineering of Light" from ICFO (The Institute of Photonic Sciences) led by Prof. Dr. Juan P. Torres tend to follow two lines of experimental research: 1) the application of the Weak Value Amplification on the Lamellar periodic dielectric waveguide structure; 2) the study of the test of the Quantum Differential Interference Contrast.

References

[1] Carl W Helstrom and Carl W Helstrom. *Quantum detection and estimation theory*. Vol. 84. Academic press New York, 1976.

[2] Yakir Aharonov; David Z. Albert; Lev Vaidman. "How the result of a measurement of a component of the spin of a spin-1/2 particle can turn out to be 100". In: *Physical Review Letters* 60.14 (1988), pp. 1351–1354. DOI: 10.1103/PhysRevLett.60.1351.

[3] I. M. Duck, P. M. Stevenson, and E. C. G. Sudarshan. "The sense in which a "weak measurement" of a spin-particle's spin component yields a value 100". In: *Phys. Rev. D* 40 (6 Sept. 1989), pp. 2112–2117. DOI: 10.1103/PhysRevD.40.2112.

[4] Yakir Aharonov and Lev Vaidman. "Properties of a quantum system during the time interval between two measurements". In: *Phys. Rev. A* 41 (1 Jan. 1990), pp. 11–20. DOI: 10.1103/PhysRevA.41.11.

[5] Justin Dressel et al. *Understanding Quantum Weak Values: Basics and Applications*. 2014. arXiv: 1305.7154 [quant-ph].

[6] Salazar-Serrano; Luis José et al. "Measurement of sub-pulse-width temporal delays via spectral interference induced by weak value amplification". In: *Phys. Rev. A* 89 (1 Jan. 2014), p. 012126. DOI: 10.1103/PhysRevA.89.012126.

[7] C. K. Hong; Z. Y. Ou and L. Mandel. "Measurement of subpicosecond time intervals between two photons by interference". In: *Phys. Rev. Lett* 59.18 (1987), pp. 2044–2046. DOI: 10.1103/PhysRevLett.59.2044.

[8] Juan Carlos Garcia-Escartin and Pedro Chamorro-Posada. "Swap test and Hong-Ou-Mandel effect are equivalent". In: *Physical Review A* 87.5 (2013), p. 052330.

[9] Walter Lang. *Nomarski differential interference-contrast microscopy*. Carl Zeiss, 1982.

[10] Przemek J.; Pavel Cheben; Alejandro Ortega-Moñux; Carlos Alonso-Ramos; Schmid Jens H.; Jean Lapointe; Dan-Xia Xu; J. Gonzalo Wangüemert-Pérez; Íñigo Molina-Fernández; Siegfried Janz Halir Robert; Bock. "Waveguide sub-wavelength structures: a review of principles and applications". In: *Laser Photonics Reviews* 9.1 (2015), pp. 25–49. DOI: https://doi.org/10.1002/lpor.201400083.

[11] O. Hosten; P. Kwiat. "Observation of the spin Hall effect of light via weak measurements". In: *Science* 319.5864 (2008), pp. 787–790. DOI: 10.1126/science.1152697.

[12] P. Ben Dixon; David J. Starling; Andrew N. Jordan; John C. Howell. "Ultrasensitive Beam Deflection Measurement via Interferometric Weak Value Amplification". In: *Physical Review Letters* 102.17 (2009). DOI: 10.1103/PhysRevLett.102.173601.

[13] Lundeen Jeff S.; Sutherland Brandon; Patel Aabid; Stewart Corey; Bamber Charles. "Direct measurement of the quantum wavefunction". In: *Nature* 474.7350 (2011), pp. 188–191. DOI: 10.1038/nature10120.

[14] L. Torres J.; Salazar-Serrano. "Weak value amplification: a view from quantum estimation theory that highlights what it is and what isn't." In: *Sci Rep* 6 (2016), p. 19702. DOI: https://doi.org/10.1038/srep19702.

[15] Dale C Flanders. "Submicrometer periodicity gratings as artificial anisotropic dielectrics". In: *Applied Physics Letters* 42.6 (1983), pp. 492–494.

[16] Philippe Lalanne; Dominique Lemercier-lalanne. "On the effective medium theory of subwavelength periodic structures". In: *J. Modern Optics* 43 (1996), pp. 2063–2085.

[17] P. A. M. Dirac. "A new notation for quantum mechanics". In: *Mathematical Proceedings of the Cambridge Philosophical Society* 35.3 (1939), pp. 416–418. DOI: 10.1017/S0305004100021162.

[18] C. Santori; D. Fattal; J. Vuckovic; G. S. Solomon and Y. Yamamoto. "Indistinguishable photons from a single-photon device". In: *419* (2002), pp. 594–597. DOI: doi:10.1038/nature01086.

[19] Radosław Chrapkiewicz et al. "Hologram of a Single Photon". In: *Nature Photonics* 10 (July 2016). DOI: 10.1038/nphoton.2016.129.